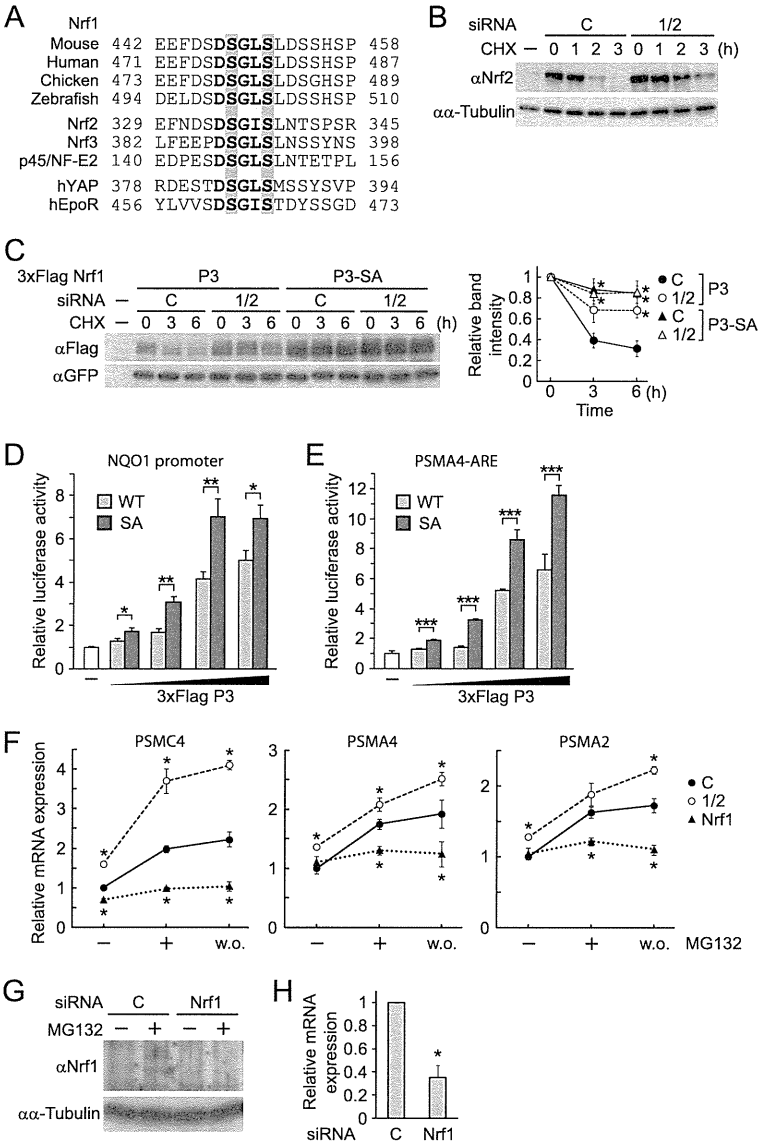

FIG. 5. A DSGLS motif is required for the β-TrCP-mediated degradation of Nrf1. (A) Alignment of Nrf1 sequences among species and NF-E2-related factors around the highly conserved DSGLS motif, which is similar to the β-TrCP recognition motifs of the human YAP and erythropoietin receptor (EpoR). Shaded areas denote conserved serine residues that were replaced with alanine for subsequent experiments. (B) β-TrCP siRNA stabilized endogenous Nrf2. Transfection of siRNA and subsequent cycloheximide chase were performed, as described in the legend to Fig. 2F. (C) Alanine substitution of serine residues in the DSGLS motif (P3-SA) stabilized the P3 Nrf1 mutant. At 48 h after transfection of siRNA and Nrf1 mutant constructs, the cycloheximide chase experiment was conducted, as described in the legend to Fig. 4B. Assays were performed three times. The values were normalized with GFP and presented as the means ± standard errors ($n = 3$; *, $P < 0.05$ versus P3 with control siRNA). (D and E) A nuclear degradation mechanism repressed the transcriptional activity of Nrf1. COS7 cells were transfected with either P3 (WT) or P3-SA (SA) Nrf1 mutant plasmid in combination with a luciferase reporter containing a single ARE of NQO1 gene (D) or three tandem copies of ARE of PSMA4 (E). The levels of luciferase activity were normalized with the *Renilla* luciferase activity of an internal control pRL-TK, and results are presented as the means ± standard deviations ($n = 3$ [D] and $n = 4$ [E]; *, $P < 0.05$; **, $P < 0.01$; ***, $P < 0.001$). (F) β-TrCP is involved in the regulation of the expression of Nrf1 target genes induced by proteasome inhibition. HeLa cells transfected twice with the indicated siRNA were left untreated (−) or were treated with (+) MG132 (1 μM) for 16 h, and then MG132-treated cells were incubated without MG132 for another 3 h (w.o.). The mRNA expression levels were determined by real-time quantitative PCR analysis. The values were normalized with 18S rRNA and are presented as the means ± standard deviations ($n = 3$; *, $P < 0.05$ versus control siRNA). (G and H) The siRNA-mediated knockdown of Nrf1. HeLa cells were twice transfected with control (C) or Nrf1 siRNA. At 24 h after the second transfection, Nrf1 knockdown efficiency was determined by immunoblot analysis with anti-Nrf1 (H-285) antibody (G) or by real-time quantitative PCR analysis (H). For immunoblot analysis, cells were treated with MG132 (10 μM) for 8 h. The values were normalized with 18S rRNA and are presented as the means ± standard deviations ($n = 4$; *, $P < 0.001$).

chase experiments. While the degradation of the P3 mutant was efficiently suppressed by siRNA-mediated β-TrCP knockdown, as expected, the P3-SA mutant was significantly stabilized even in the absence of β-TrCP siRNA (Fig. 5C). Thus, these data clearly indicate that the DSGLS motif is required for the β-TrCP-mediated degradation of Nrf1.

β-TrCP-mediated degradation represses the transcriptional activity of Nrf1. The involvement of β-TrCP in the regulation of Nrf1 stability prompted us to investigate the effect of the knockdown of β-TrCP on the transcriptional activity of Nrf1. The ubiquitin-proteasome pathway has been reported to activate transcription by regulating a variety of transcriptional factors (15, 19). Our hypothesis was that a nuclear degradation mechanism is required to achieve Nrf1-mediated transcription after its activation. To test our hypothesis, we compared the transcriptional activity of the P3 and P3-SA mutants in a luciferase reporter assay using COS7 cells. We first utilized a luciferase reporter driven by the NQO1 promoter, which contained the Nrf1 recognition sequence ARE (9). Forced expression of the P3 mutant increased reporter activity in a dose-dependent manner (Fig. 5D), indicating that this mutant retains transcriptional activity. Notably, the P3-SA mutant exhibited enhanced transcriptional activity compared with that of the P3 mutant (Fig. 5D). This result suggests that β-TrCP-mediated degradation of Nrf1 is involved in the repression of Nrf1-dependent transcription. Recent reports have indicated that Nrf1 regulates the expression of a set of proteasome subunit genes in response to the proteasome inhibition (27, 31). We then utilized another luciferase reporter that contains three copies of the ARE of the PSMA4 promoter (27). The result was similar to that obtained with the NQO1 promoter (Fig. 5E). To further clarify the role of β-TrCP in Nrf1-mediated transcription, we examined the effect of β-TrCP knockdown on the expression of endogenous proteasome subunit genes induced by proteasome inhibition. The expression of PSMC4, PSMA4, and PSMA2 was induced by the treatment of HeLa cells with MG132 for 16 h, and this induction was significantly repressed by the siRNA knockdown of Nrf1 (Fig. 5F, Nrf1 and C). Efficient silencing of Nrf1 was confirmed at both the protein and the mRNA levels (Fig. 5G and H). This result indicates that the induction of these genes is highly dependent on Nrf1. Under this situation, the siRNA knockdown of β-TrCP significantly enhanced the expression of PSMC4, PSMA4, and PSMA2 induced by MG132 (Fig. 5F, 1/2 and C). This enhancement persisted after the washing out of MG132. These results clearly demonstrate that β-TrCP is involved in the repression of the transcriptional activation of Nrf1 target genes such as the proteasome subunit genes.

Hrd1 and VCP mediate the cytoplasmic degradation of Nrf1. We investigated the molecular mechanism underlying the cytoplasmic degradation of Nrf1. In keeping with a recent report demonstrating that Nrf1 is degraded via the ERAD pathway (31), the siRNA knockdown of VCP, an AAA-ATPase required for protein transport from the ER to the proteasome during ERAD, increased the quantity of the endogenous Nrf1 protein in HeLa cells (Fig. 6A). In addition, among several ERAD-related E3 ligases, the knockdown of Hrd1 specifically increased the expression of the Nrf1 protein. The efficient silencing of these genes was confirmed by a real-time quantitative PCR analysis (Fig. 6B). A cycloheximide chase experiment further revealed that the knockdown of VCP or Hrd1 significantly stabilized the Nrf1 protein (Fig. 6C). Notably, the electrophoretic mobility of Nrf1 was altered by the knockdown of VCP or Hrd1, suggesting that the limited proteolysis and/or posttranslational modification of Nrf1 was impaired (see Discussion). The knockdown of other ERAD E3 ligases, gp78 and TEB4, did not stabilize Nrf1 (Fig. 6C). These results indicate that Nrf1 undergoes cytoplasmic degradation via the Hrd1-dependent ERAD pathway.

We next investigated whether transcriptional activity of Nrf1 is suppressed by cytoplasmic degradation via the ERAD pathway. We examined the effect of siRNA knockdown of Hrd1 on the expression of Nrf1 target genes. The result shows that siRNA against Hrd1 as well as β-TrCP significantly enhanced proteasome subunit gene expression, suggesting that cytoplasmic degradation functions to suppress Nrf1 activity (Fig. 6D).

An amino acid region (residues 31 to 81) is required for the cytoplasmic degradation of Nrf1. Finally, we attempted to identify an amino acid region responsible for the cytoplasmic degradation of Nrf1. As demonstrated in Fig. 2, the ΔbZip Nrf1 mutant that localized in the cytoplasm was degraded in a β-TrCP-independent manner. Accordingly, we first generated two ΔbZip mutants, one lacking the N-terminal region (ΔbZip-1) and the other lacking the Neh2L domain, which shares considerable homology with the Keap1-interacting domain in Nrf2 (ΔbZip-2) (Fig. 6E). Immunocytochemical staining confirmed the predominant cytoplasmic localization of the mutants (data not shown). The stability of these mutant proteins was determined by a cycloheximide chase experiment. As a result, significant stabilization of the ΔbZip mutant was observed when its N-terminal region was deleted (Fig. 6F, ΔbZip-1), implying that this region is required for the cytoplasmic degradation of Nrf1. In contrast, the deletion of the Neh2L domain did not affect the stability of the ΔbZip mutant (Fig. 6F, ΔbZip-2), reemphasizing that Keap1 is not involved in the cytoplasmic degradation of Nrf1. We further introduced a series of deletions in the N-terminal region of the ΔbZip mutant and analyzed the stability of these mutants (Fig. 6E, ΔbZip-3 to ΔbZip-6). Deletion of either the NHB1 domain or the NHB2 domain did not alter the stability of the ΔbZip mutant protein (Fig. 6G, ΔbZip-3 and ΔbZip-5). In contrast, the deletion of a short region (residues 31 to 81) located between the NHB1 and NHB2 domains markedly stabilized the ΔbZip mutant protein (Fig. 6G, ΔbZip-4 and ΔbZip-6). These results indicate that the region in question (residues 31 to 81) is required for the cytoplasmic degradation of Nrf1. The genome database indicates that this region is highly conserved among species and is partially conserved in Nrf3, thereby suggesting its functional significance in the degradation of Nrf1 (Fig. 6H). Taken together, our data indicate that the cytoplasmic degradation of Nrf1 is regulated by a small region between the NHB1 and NHB2 domains, which is not associated with the β-TrCP-mediated degradation of Nrf1.

DISCUSSION

In this study, we investigated the mechanisms by which the transcriptional activity of Nrf1 is modulated to sustain cellular homeostasis. We determined that β-TrCP- and Hrd1-dependent degradation mechanisms regulate the biological activity

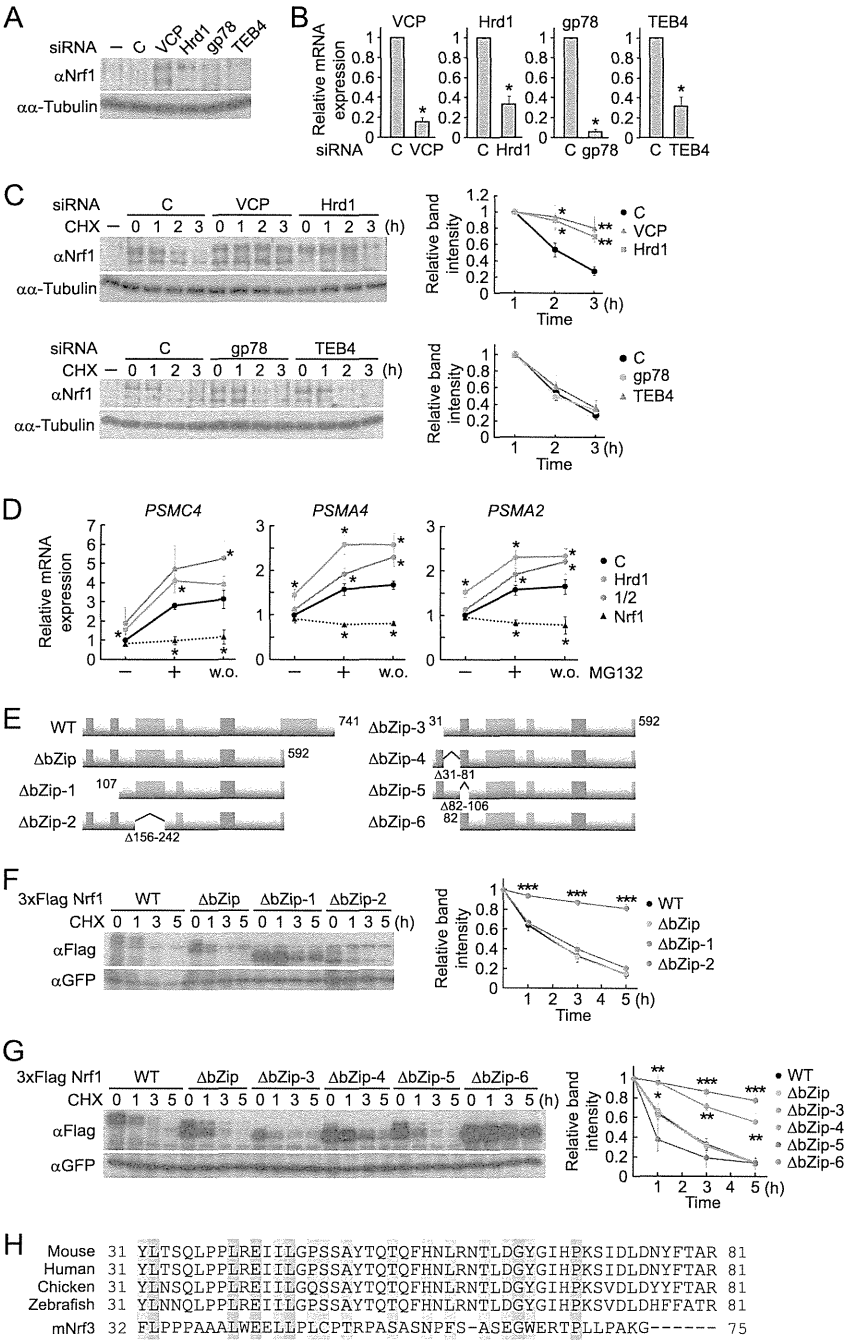

FIG. 6. Hrd1 and VCP regulate the cytoplasmic degradation of Nrf1. (A) VCP or Hrd1 siRNA stabilized endogenous Nrf1 in HeLa cells. Transfection was carried out twice. The whole-cell extracts were prepared and analyzed by immunoblotting with anti-Nrf1 (H-285) antibody. α-Tubulin is an internal control. (B) Knockdown efficiency of ERAD-related E3 ligases. A knockdown experiment was conducted as described in the legend to Fig. 5H. The values were normalized with 18S rRNA and are presented as the means ± standard deviations ($n = 4$; *, $P < 0.001$). (C) Knockdown of VCP and Hrd1 inhibited Nrf1 degradation. Transfection of siRNA and subsequent cycloheximide chase were performed, as described in the legend to Fig. 2F. Data are presented as the means ± standard errors ($n = 5$; *, $P < 0.05$; **, $P < 0.01$ versus control siRNA). (D) Hrd1 is involved in the regulation of the expression of Nrf1 target genes induced by proteasome inhibition. The assays were performed according to the legend of Fig. 5F. Data are presented as the means ± standard deviations ($n = 3$; *, $P < 0.05$ versus control siRNA). (E) Schematic structures of deletion mutants derived from the ΔbZip Nrf1 mutant. (F and G) A region (residues 31 to 81) of Nrf1 is required for the cytoplasmic degradation of Nrf1. Cycloheximide chase experiments using the Nrf1 deletion mutants were performed according to the legend of Fig. 4B. Data are presented as the means ± standard errors ($n = 7$ [F]; $n \geq 3$ [G]; *, $P < 0.05$; **, $P < 0.005$; ***, $P < 0.001$ versus wild-type Nrf1). (H) Amino acid residues (31 to 81) of mouse Nrf1 are highly conserved among species and in mouse Nrf3 (mNrf3). Shaded amino acid positions highlight amino acid identity (orange) or similarity (blue) between Nrf1 and Nrf3.

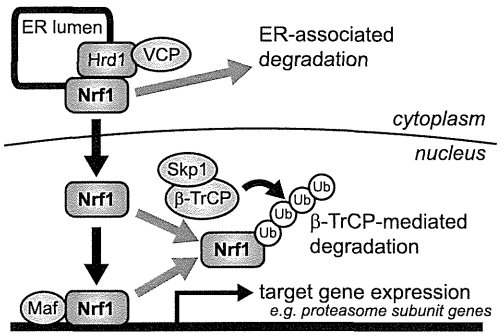

FIG. 7. A model for the dual mechanisms of Nrf1 degradation in regulating the expression of Nrf1 target genes. Nrf1 is degraded via the ERAD pathway under physiological conditions. Upon activation, Nrf1 is stabilized and translocates into the nucleus. In the nucleus, β-TrCP-mediated degradation prevents inappropriate transcription of Nrf1 target genes such as proteasome subunit genes. This degradation may also facilitate the clearance of Nrf1 from the nucleus after the activation of Nrf1 is abolished. Ub, ubiquitin.

of Nrf1 in the nucleus and the cytoplasm, respectively. Under homeostatic conditions, Nrf1 is sequestered in the ER through its NHB1 domain and undergoes proteasomal degradation in an Hrd1-dependent manner. Upon exposure to activating signals, Nrf1 evades degradation and activates expression of its target genes. After Nrf1 produces biological responses, its activity is terminated by the β-TrCP-dependent degradation process. Also, this study is the first to demonstrate that β-TrCP is involved in the regulation of proteasome subunit gene expression. Our schematic model in Fig. 7 summarizes the regulatory mechanism of Nrf1, which is tightly coupled with two distinct degradation pathways.

Multiple lines of evidence suggest that a cytoprotection system is a double-edged sword; specifically, constitutive activation of the system rather alters homeostatic balances (16). For example, our group and other investigators have identified that the aberrant activation of the oxidative stress response by somatic mutations to the *NRF2* and *KEAP1* genes provides growth advantages and anticancer drug resistance to human lung cancer cells (22, 24, 29, 30). These findings strongly suggest that the precise repression of the stress response system under nonstressed conditions is also indispensable for cellular homeostasis. In this regard, two discrete proteolysis pathways contribute to the suppression of the inappropriate activation of Nrf1. The cytoplasmic degradation mechanism achieves the complete repression of Nrf1 activity, as well as its retention in the ER. Moreover, the nuclear degradation pathway also prevents unnecessary expression of Nrf1 target genes under physiological conditions and may resolve the gene activation after stress termination. Given that Nrf1 upregulates expression of proteasome subunit genes in response to proteasome inhibition, two distinct degradation mechanisms should strictly regulate Nrf1 activity to maintain proteasome homeostasis.

We identified the DSGLS motif in Nrf1. This motif resembles the canonical β-TrCP recognition sequence (DpSGX$_n$pS), and similar sequences are found in EpoR and the transcriptional coactivator YAP (17, 43). The DSGX$_n$S motif usually requires phosphorylation to associate with β-TrCP. In fact, alanine substitutions at the conserved serine residues (Ser448 and Ser451) in the Nrf1 P3 mutant markedly compromised the β-TrCP-dependent degradation of Nrf1 (Fig. 5C). This finding suggests the involvement of the phosphorylation of the DSGLS motif in the β-TrCP-dependent degradation of Nrf1. We found that lithium chloride (LiCl), a potent but nonselective GSK-3 inhibitor, slightly stabilized Nrf1; however, SB216763, a more selective inhibitor of GSK-3, did not (data not shown). Thus, further analyses are required to identify the kinase(s) responsible for the phosphorylation of the DSGLS motif and the regulatory mechanism of the nuclear degradation of Nrf1. Because the DSGLS motif is highly conserved in NF-E2-related factors (p45/NF-E2, Nrf1, Nrf2, and Nrf3), the β-TrCP-mediated degradation mechanism might be a common regulatory pathway among these transcription factors. In accordance with our result, a study published during the preparation of the manuscript demonstrated that Nrf2 possesses the DSGLS motif and is degraded by β-TrCP in a Keap1-independent manner (26). Thus, unlike Keap1, β-TrCP might be a common factor in the repression of the gene expression induced by NF-E2-related factors.

We do not exclude the possibility that β-TrCP is positively involved in transcriptional activation by Nrf1. As shown in Fig. 5C to E, the transcriptional activity of the P3-SA mutant was not strongly increased, in spite of its significant stabilization. This finding may indicate that β-TrCP-mediated proteolysis contributes to both the resolution and the activation of transcriptional processes by Nrf1. Multiple lines of evidence suggest that the ubiquitin-proteasome pathway can activate transcription by regulating a variety of transcriptional factors (15, 19). For instance, the F-box protein Fbw7a promotes degradation of the steroid receptor coactivator SRC-3, consequently increasing the turnover of SRC-3 on the promoters of target genes and activating their transcription. Alternatively, the cooperative interaction of β-TrCP with the transcriptional coactivator p300/CBP enhances the expression of β-catenin-regulated genes (11). Because CBP activates the transcriptional activity of Nrf1 via the Neh5L domain (39), β-TrCP may synergistically recruit p300/CBP on Nrf1 and promote transcriptional activation by Nrf1 as well as its proteolysis.

A remaining important issue regarding the biological function of Nrf1 is the mechanism by which Nrf1 is liberated from ER sequestration and then activates gene expression. In this regard, we consider two possibilities. First, the inhibition of Hrd1-mediated degradation in the cytoplasm may lead to the nuclear translocation of Nrf1. We observed that MG132 treatment promotes the nuclear accumulation of the endogenous Nrf1 in MEFs and HeLa cells (Fig. 1A and data not shown). In addition, Nrf1 has been reported to mediate the induction of proteasome subunit genes after proteasome inhibition in mammalian cells (27, 31). These results imply that the suppression of cytoplasmic degradation allows Nrf1 to translocate into the nucleus and activate gene expression. In this hypothetical model, Nrf1 would function to recover proteasome activity by upregulating expression of proteasome subunit genes under a situation of proteasome dysfunction. Our current study determined that the cytoplasmic stability of Nrf1 is modulated by the ERAD-related ubiquitin ligase Hrd1 and VCP (Fig. 6A and C). Although the regulatory mechanisms of the Hrd1- and VCP-mediated proteasomal degradation pathways remain ob-

scure, further analysis might demonstrate that the inhibition of cytoplasmic degradation is the mechanism of Nrf1 activation.

A second possibility is that proteolytic cleavage may release Nrf1 from ER sequestration. For example, the ER-embedded transcription factors ATF-6 and SREBP (sterol regulatory element binding protein) translocate to the Golgi compartment in response to activating signals and are sequentially cleaved by Site-1 and Site-2 proteases, thereby resulting in their nuclear entry and their activation of target genes (2, 18). Indeed, we found that nuclearly accumulated Nrf1 migrated slightly more quickly than its cytoplasmically localized form in the gels (Fig. 1A). In addition, silencing of VCP and Hrd1 altered the electrophoretic mobility of Nrf1 (Fig. 6C). These results suggest that the cleavage of Nrf1 is also essential for its liberation from the ER. In this model, Hrd1 may eliminate the ER-accumulated Nrf1 that is not cleaved by a protease under nonstress conditions. To examine our two current hypotheses, further proteomics-based or genetic experiments to identify Nrf1-associated molecules may shed light on this issue.

Discussing the Nrf1 degradation mechanism from the perspective of molecular evolution would be interesting. The transcription factors *Caenorhabditis elegans* Skn-1 and *Drosophila* CncC are considered to be ancestral genes of NF-E2-related factors and activate the expression of oxidative stress response genes (32). Intriguingly, both factors are also regulated by proteasomal degradation (4, 6, 25). For instance, Skn-1 is degraded through polyubiquitination by the WDR-23/Cul4/DDB1 ubiquitin ligase under physiological conditions (4). Exhibiting similarity to the structure of β-TrCP, WDR-23 contains a WD40 repeat domain and functions as a ubiquitin ligase adaptor. The degradation process of Skn-1 is mediated by the p38 mitogen-activated protein (MAP) kinase, GSK-3, and the insulin-like receptor pathways, suggesting the presence of phosphorylation-dependent regulation. CncC is controlled by both Keap1-dependent and -independent proteasomal pathways (6). Notably, CncC also regulates the gene expression of proteasome subunits. Because Skn-1 and CncC do not possess the DSGLS motif, β-TrCP may not be involved in the regulation of these factors. Nevertheless, these transcription factors share the characteristic that their transcriptional activities are regulated by the ubiquitin-proteasome system. We surmise that the NF-E2-related factors underwent molecular evolution from these ancestral genes by acquiring the DSGLS motif and subsequently switching to the β-TrCP-mediated regulatory system. Such an evolutionary process may have conferred biological diversity and complexity to these transcription factors.

ACKNOWLEDGMENTS

We are grateful to Keiko Nakayama, Raymond J. Deshaies, and Dirk Bohmann for the β-TrCP2 plasmids, 3×PSMA4-ARE-Luc, and HA ubiquitin, respectively. We also thank Tomoki Chiba, Takako Tsukide, Akiko Matsumoto, and Jun Takai for research support.

This work was supported in part by grants-in-aid from the Ministry of Education, Sports, Science and Technology (A.K., Y.T., and M.Y.), the Mochida Memorial Foundation (A.K.), the Naito Foundation (A.K.), the Suzuken Memorial Foundation (A.K.), the Takeda Science Foundation (A.K.), the Inamori Foundation (Y.T.), and the Uehara Memorial Foundation (Y.T.).

REFERENCES

1. **Bagola, K., M. Mehnert, E. Jarosch, and T. Sommer.** 2011. Protein dislocation from the ER. Biochim. Biophys. Acta **1808:**925–936.
2. **Brown, M. S., J. Ye, R. B. Rawson, and J. L. Goldstein.** 2000. Regulated intramembrane proteolysis: a control mechanism conserved from bacteria to humans. Cell **100:**391–398.
3. **Chan, J. Y., et al.** 1998. Targeted disruption of the ubiquitous CNC-bZIP transcription factor, Nrf-1, results in anemia and embryonic lethality in mice. EMBO J. **17:**1779–1787.
4. **Choe, K. P., A. J. Przybysz, and K. Strange.** 2009. The WD40 repeat protein WDR-23 functions with the CUL4/DDB1 ubiquitin ligase to regulate nuclear abundance and activity of SKN-1 in *Caenorhabditis elegans*. Mol. Cell. Biol. **29:**2704–2715.
5. **Frescas, D., and M. Pagano.** 2008. Deregulated proteolysis by the F-box proteins SKP2 and β-TrCP: tipping the scales of cancer. Nat. Rev. Cancer **8:**438–449.
6. **Grimberg, K. B., A. Beskow, D. Lundin, M. M. Davis, and P. Young.** 2011. Basic-leucine zipper protein Cnc-C is a substrate and transcriptional regulator of the *Drosophila* 26S proteasome. Mol. Cell. Biol. **31:**897–909.
7. **Hershko, A.** 2005. The ubiquitin system for protein degradation and some of its roles in the control of the cell-division cycle (Nobel lecture). Angew. Chem. Int. Ed. Engl. **44:**5932–5943.
8. **Hosokawa, N., Y. Kamiya, and K. Kato.** 2010. The role of MRH domain-containing lectins in ERAD. Glycobiology **20:**651–660.
9. **Kang, M. I., A. Kobayashi, N. Wakabayashi, S. G. Kim, and M. Yamamoto.** 2004. Scaffolding of Keap1 to the actin cytoskeleton controls the function of Nrf2 as key regulator of cytoprotective phase 2 genes. Proc. Natl. Acad. Sci. U. S. A. **101:**2046–2051.
10. **Kim, J., W. Xing, J. Wergedal, J. Y. Chan, and S. Mohan.** 2010. Targeted disruption of nuclear factor erythroid-derived 2-like 1 in osteoblasts reduces bone size and bone formation in mice. Physiol. Genomics **40:**100–110.
11. **Kimbrel, E. A., and A. L. Kung.** 2009. The F-box protein β-TrCp1/Fbw1a interacts with p300 to enhance β-catenin transcriptional activity. J. Biol. Chem. **284:**13033–13044.
12. **Kobayashi, A., et al.** 2006. Oxidative and electrophilic stresses activate Nrf2 through inhibition of ubiquitination activity of Keap1. Mol. Cell. Biol. **26:**221–229.
13. **Kobayashi, A., et al.** 2011. Central nervous system-specific deletion of transcription factor Nrf1 causes progressive motor neuronal dysfunction. Genes Cells **16:**692–703.
14. **Kobayashi, M., and M. Yamamoto.** 2006. Nrf2-Keap1 regulation of cellular defense mechanisms against electrophiles and reactive oxygen species. Adv. Enzyme Regul. **46:**113–140.
15. **Lonard, D. M., and B. W. O'Malley.** 2008. SRC-3 transcription-coupled activation, degradation, and the ubiquitin clock: is there enough coactivator to go around in cells? Sci. Signal. **1:**pe16.
16. **Luo, J., N. L. Solimini, and S. J. Elledge.** 2009. Principles of cancer therapy: oncogene and non-oncogene addiction. Cell **136:**823–837.
17. **Meyer, L., et al.** 2007. β-Trcp mediates ubiquitination and degradation of the erythropoietin receptor and controls cell proliferation. Blood **109:**5215–5222.
18. **Mori, K.** 2003. Frame switch splicing and regulated intramembrane proteolysis: key words to understand the unfolded protein response. Traffic **4:**519–528.
19. **Muratani, M., and W. P. Tansey.** 2003. How the ubiquitin-proteasome system controls transcription. Nat. Rev. Mol. Cell Biol. **4:**192–201.
20. **Nakayama, K. I., and K. Nakayama.** 2006. Ubiquitin ligases: cell-cycle control and cancer. Nat. Rev. Cancer **6:**369–381.
21. **Natsume, T., et al.** 2002. A direct nanoflow liquid chromatography-tandem mass spectrometry system for interaction proteomics. Anal. Chem. **74:**4725–4733.
22. **Ohta, T., et al.** 2008. Loss of Keap1 function activates Nrf2 and provides advantages for lung cancer cell growth. Cancer Res. **68:**1303–1309.
23. **Ohtsuji, M., et al.** 2008. Nrf1 and Nrf2 play distinct roles in activation of antioxidant response element-dependent genes. J. Biol. Chem. **283:**33554–33562.
24. **Padmanabhan, B., et al.** 2006. Structural basis for defects of Keap1 activity provoked by its point mutations in lung cancer. Mol. Cell **21:**689–700.
25. **Page, B. D., S. J. Diede, J. R. Tenlen, and E. L. Ferguson.** 2007. EEL-1, a Hect E3 ubiquitin ligase, controls asymmetry and persistence of the SKN-1 transcription factor in the early *C. elegans* embryo. Development **134:**2303–2314.
26. **Rada, P., et al.** 2011. SCF/β-TrCP promotes glycogen synthase kinase 3-dependent degradation of the Nrf2 transcription factor in a Keap1-independent manner. Mol. Cell. Biol. **31:**1121–1133.
27. **Radhakrishnan, S. K., et al.** 2010. Transcription factor Nrf1 mediates the proteasome recovery pathway after proteasome inhibition in mammalian cells. Mol. Cell **38:**17–28.
28. **Ravid, T., and M. Hochstrasser.** 2008. Diversity of degradation signals in the ubiquitin-proteasome system. Nat. Rev. Mol. Cell Biol. **9:**679–690.
29. **Shibata, T., et al.** 2008. Cancer related mutations in *NRF2* impair its recog-

nition by Keap1-Cul3 E3 ligase and promote malignancy. Proc. Natl. Acad. Sci. U. S. A. **105:**13568–13573.
30. **Singh, A., et al.** 2006. Dysfunctional KEAP1-NRF2 interaction in non-small-cell lung cancer. PLoS Med. **3:**e420.
31. **Steffen, J., M. Seeger, A. Koch, and E. Kruger.** 2010. Proteasomal degradation is transcriptionally controlled by TCF11 via an ERAD-dependent feedback loop. Mol. Cell **40:**147–158.
32. **Sykiotis, G. P., and D. Bohmann.** 2010. Stress-activated cap'n'collar transcription factors in aging and human disease. Sci. Signal. **3:**re3.
33. **Treier, M., L. M. Staszewski, and D. Bohmann.** 1994. Ubiquitin-dependent c-Jun degradation in vivo is mediated by the delta domain. Cell **78:**787–798.
34. **Wang, W., and J. Y. Chan.** 2006. Nrf1 is targeted to the endoplasmic reticulum membrane by an N-terminal transmembrane domain. Inhibition of nuclear translocation and transacting function. J. Biol. Chem. **281:**19676–19687.
35. **Watai, Y., et al.** 2007. Subcellular localization and cytoplasmic complex status of endogenous Keap1. Genes Cells **12:**1163–1178.
36. **Xing, W., et al.** 2007. Nuclear factor-E2-related factor-1 mediates ascorbic acid induction of osterix expression via interaction with antioxidant-responsive element in bone cells. J. Biol. Chem. **282:**22052–22061.
37. **Xu, Z., et al.** 2005. Liver-specific inactivation of the Nrf1 gene in adult mouse leads to nonalcoholic steatohepatitis and hepatic neoplasia. Proc. Natl. Acad. Sci. U. S. A. **102:**4120–4125.
38. **Yamasaki, S., et al.** 2007. Cytoplasmic destruction of p53 by the endoplasmic reticulum-resident ubiquitin ligase "Synoviolin." EMBO J. **26:**113–122.
39. **Zhang, J., et al.** 2007. Nrf2 Neh5 domain is differentially utilized in the transactivation of cytoprotective genes. Biochem. J. **404:**459–466.
40. **Zhang, Y., D. H. Crouch, M. Yamamoto, and J. D. Hayes.** 2006. Negative regulation of the Nrf1 transcription factor by its N-terminal domain is independent of Keap1: Nrf1, but not Nrf2, is targeted to the endoplasmic reticulum. Biochem. J. **399:**373–385.
41. **Zhang, Y., J. M. Lucocq, and J. D. Hayes.** 2009. The Nrf1 CNC/bZIP protein is a nuclear envelope-bound transcription factor that is activated by t-butyl hydroquinone but not by endoplasmic reticulum stressors. Biochem. J. **418:**293–310.
42. **Zhang, Y., J. M. Lucocq, M. Yamamoto, and J. D. Hayes.** 2007. The NHB1 (N-terminal homology box 1) sequence in transcription factor Nrf1 is required to anchor it to the endoplasmic reticulum and also to enable its asparagine-glycosylation. Biochem. J. **408:**161–172.
43. **Zhao, B., L. Li, K. Tumaneng, C. Y. Wang, and K. L. Guan.** 2010. A coordinated phosphorylation by Lats and CK1 regulates YAP stability through $SCF^{\beta\text{-}TRCP}$. Genes Dev. **24:**72–85.
44. **Zhao, R., et al.** 2011. Long isoforms of NRF1 contribute to arsenic-induced antioxidant response in human keratinocytes. Environ. Health Perspect. **119:**56–62.

Intracellular phosphatidylserine is essential for retrograde membrane traffic through endosomes

Yasunori Uchida[a,1], Junya Hasegawa[a,1], Daniel Chinnapen[b], Takao Inoue[a], Seiji Okazaki[c], Ryuichi Kato[c], Soichi Wakatsuki[c], Ryo Misaki[d], Masato Koike[e], Yasuo Uchiyama[e], Shun-ichiro Iemura[f], Tohru Natsume[f], Ryusuke Kuwahara[g], Takatoshi Nakagawa[h], Kiyotaka Nishikawa[i], Kojiro Mukai[a], Eiji Miyoshi[j], Naoyuki Taniguchi[k], David Sheff[l], Wayne I. Lencer[b], Tomohiko Taguchi[a,2], and Hiroyuki Arai[a,2]

[a]Department of Health Chemistry, Graduate School of Pharmaceutical Sciences, University of Tokyo, Tokyo 113-0033, Japan; [b]Department of Gastrointestinal Cell Biology, Children's Hospital and Department of Pediatrics, Harvard Medical School, Boston, MA 02115; [c]Structural Biology Research Center, Photon Factory, Institute of Materials Structure Science, High Energy Accelerator Research Organization (KEK), Tsukuba, Ibaraki 305-0801, Japan; [d]International Center for Biotechnology, Osaka University, 2-1 Yamadaoka, Suita, Osaka 565-0871, Japan; [e]Department of Cell Biology and Neuroscience, Juntendo University School of Medicine, Tokyo 113-8421, Japan; [f]Biomedicinal Information Research Center, National Institute of Advanced Industrial Science and Technology, 2-4-7 Aomi, Koto-ku, Tokyo 135-0064, Japan; [g]Department of Biochemistry, Osaka University Graduate School of Medicine, Osaka 565-0871, Japan; [h]Department of Pharmacology, Osaka Medical College, Takatsuki, Osaka 569-8686, Japan; [i]Faculty of Life and Medical Sciences, Doshisha University, Kyoto 610-0394, Japan; [j]Department of Molecular Biochemistry and Clinical Investigation, Division of Health Science, Osaka University Graduate School of Medicine, Osaka 565-0871, Japan; [k]Systems Glycobiology Research Group, Advanced Science Institute, RIKEN, Wako, Saitama 351-0198, Japan; and [l]Department of Pharmacology, Carver College of Medicine, University of Iowa, Iowa City, IA 52242

Edited* by Kai Simons, Max Planck Institute of Molecular Cell Biology and Genetics, Dresden, Germany, and approved August 10, 2011 (received for review June 6, 2011)

Phosphatidylserine (PS) is a relatively minor constituent of biological membranes. Despite its low abundance, PS in the plasma membrane (PM) plays key roles in various phenomena such as the coagulation cascade, clearance of apoptotic cells, and recruitment of signaling molecules. PS also localizes in endocytic organelles, but how this relates to its cellular functions remains unknown. Here we report that PS is essential for retrograde membrane traffic at recycling endosomes (REs). PS was most concentrated in REs among intracellular organelles, and evectin-2 (evt-2), a protein of previously unknown function, was targeted to REs by the binding of its pleckstrin homology (PH) domain to PS. X-ray analysis supported the specificity of the binding of PS to the PH domain. Depletion of evt-2 or masking of intracellular PS suppressed membrane traffic from REs to the Golgi. These findings uncover the molecular basis that controls the RE-to-Golgi transport and identify a unique PH domain that specifically recognizes PS but not polyphosphoinositides.

cholera toxin | endocytosis

Phosphatidylserine (PS) is an anionic phospholipid class in eukaryotic biomembranes. PS is highly enriched in the plasma membrane (PM) and plays key roles in various physiological processes such as the coagulation cascade, recruitment and activation of signaling molecules, and clearance of apoptotic cells (1). These functions of PS are known to be executed by a number of proteins that have PS-recognition modules, such as a gamma-carboxyglutamic acid domain in prothrombin (2), a C2 domain in protein kinase C (3), a discoidin-type C2 domain in lactadherin (4), and a kinase associated-1 domain in MARK/PAR1 kinases (5). PS is also found in endocytic organelles (4, 6), where its functions are largely unknown.

Proteins newly synthesized at the endoplasmic reticulum (ER) that are destined for secretion or for residence within organelles move through the Golgi to their final destinations (7). This membrane outflow is counteracted by retrograde membrane flow that originates from either the PM or the endosomal system (8). The retrograde membrane traffic to the Golgi is used by several Golgi proteins to maintain their predominant Golgi localization, such as mannose 6-phosphate receptors (acid-hydrolase receptors), furin (a transmembrane enzyme), TGN38/46 (*trans*-Golgi resident proteins), and Wntless (a sorting receptor for Wnt) (9, 10). Intriguingly, some protein toxins produced by bacteria and plants, e.g., cholera toxin, Shiga toxin, and ricin, highjack this retrograde traffic to reach the cytosol, where they exert their toxicity (11, 12). The retrograde membrane traffic from the PM to the Golgi is known to pass through early endosomes (EEs)/recycling endosomes (REs) (10, 13). The molecular mechanism underlying this traffic has just begun to be elucidated (8, 9).

Here we report that PS is essential for retrograde membrane traffic at REs. PS was most concentrated in REs among intracellular organelles, and evectin-2 (evt-2), a protein of previously unknown function, was targeted to REs by the binding of its pleckstrin homology (PH) domain to PS. Depletion of evt-2 or masking of intracellular PS suppressed membrane traffic from REs to the Golgi. These findings uncover the molecular basis that controls the retrograde transport through REs, and identify a PH domain that specifically recognizes PS.

Results and Discussion

Evectin-1 (evt-1) and -2 are identified as post-Golgi proteins of unknown function (14) that have a PH domain that typically binds polyphosphoinositides (15). Evt-2 is expressed in a broad range of tissues, whereas evt-1 is expressed specifically in the nervous system. We first examined the subcellular localization of evt-2 using COS-1 cells in which organelles are spatially well separated (16, 17) (Fig. S1). Evt-2 colocalized with an RE marker, transferrin receptor (TfnR), but not with a Golgi marker (GM130), a lysosomal marker (LAMP1), or an early endosomal marker (VPS26) (Fig. 1*A*, for quantification see Fig. S2*A*). By immunoelectron microscopy using ultrathin cryosections, GFP–evt-2 (labeled with 10 nm gold particles) was specifically detected in tubulovesicular structures, and TfnR (labeled with 5 nm gold particles) was detected in some of them (Fig. 1*B* and Fig. S3). We thus concluded that evt-2 is localized predominantly to REs.

Author contributions: T.I., R. Kato, S.W., T. Natsume, E.M., N.T., W.I.L., T.T., and H.A. designed research; Y. Uchida, J.H., D.C., S.O., R.M., M.K., S.-i.I., R. Kuwahara, T. Nakagawa, K.N., K.M., D.S., and T.T. performed research; S.-i.I. and T. Natsume contributed new reagents/analytic tools; Y. Uchida, J.H., R.M., and Y. Uchiyama analyzed data; and T.T. and H.A. wrote the paper.

The authors declare no conflict of interest.

*This Direct Submission article had a prearranged editor.

Freely available online through the PNAS open access option.

Data deposition: The coordinates and structure factors have been deposited in the Protein Data Bank, www.pdb.org (PDB ID code 3AJ4).

[1]Y. Uchida and J.H. contributed equally to this work.

[2]To whom correspondence may be addressed. E-mail: tom_taguchi@mol.f.u-tokyo.ac.jp or harai@mol.f.u-tokyo.ac.jp.

This article contains supporting information online at www.pnas.org/lookup/suppl/doi:10.1073/pnas.1109101108/-/DCSupplemental.

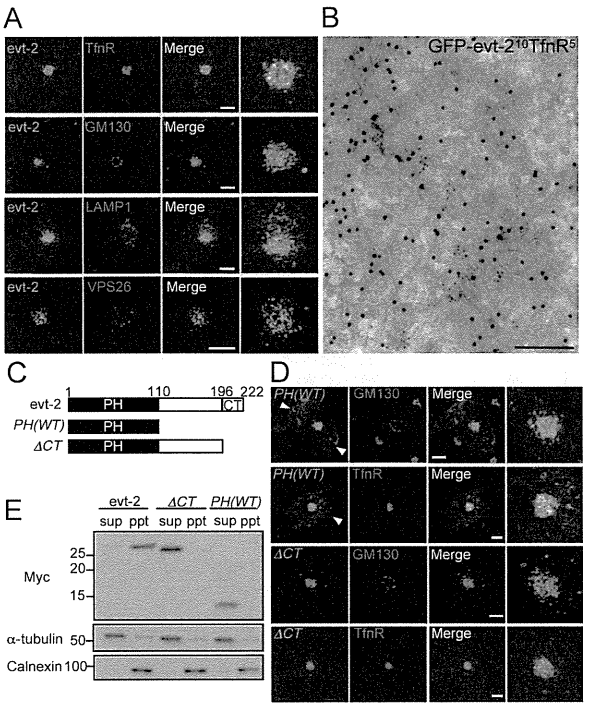

Fig. 1. A PH-domain–containing protein, evt-2, localizes to REs. (*A*) Evt-2 tagged with Myc was transiently expressed in COS-1 cells. The cells were then fixed and stained for Myc, TfnR, GM130, LAMP1, and VPS26. Magnified images around the Golgi/REs region are shown in the *Right* column. (Scale bars, 10 μm.) (*B*) Electron micrograph of an ultrathin cryosection of COS-1 cells. Cells expressing GFP–evt-2 were labeled with antibodies against GFP (10 nm in diameter) and TfnR (5 nm in diameter). (Scale bar, 250 nm.) (*C*) Domain structures of evt-2 and its truncation mutants. Myc-epitope was added to all of the constructs at the N terminus. (*D*) *PH(WT)* and *ΔCT* were transiently expressed. The cells were then fixed and stained for Myc, GM130, and TfnR. Arrowheads indicate PM. (Scale bars, 10 μm.) (*E*) Evt-2, *ΔCT*, and *PH(WT)* were transiently expressed in COS-1 cells for 24 h. Cell lysates were spun at 100,000 *g* for 60 min at 4 °C, and the resultant supernatant (sup) and pellet (ppt) were immunoblotted with anti-Myc antibody. α-Tubulin and calnexin were immunoblotted as a control.

Evt-2 also colocalized with the RE marker TfnR in HeLa cells (Fig. S4*A*).

Evt-2 has an N-terminal PH domain and a C-terminal hydrophobic region (CT) (Fig. 1*C*). *PH(WT)*, a Myc-tagged evt-2 PH domain, was targeted to REs and to the PM to some extent (Fig. 1*D*). The PH domain is thus sufficient for evt-2 targeting to REs. *ΔCT* was exclusively localized to REs as evt-2, suggesting that the domain between PH and CT constrains the RE localization of evt-2. Evt-2 was recovered in the pellet after ultracentrifugation of cell lysate, whereas truncation mutants (*ΔCT* and *PH(WT)*) were found in the supernatant (Fig. 1*E*), showing that CT is required for evt-2 association with membranes.

The human proteome has ~300 proteins with PH domains. About 10% of these proteins bind specifically to phosphatidylinositol phosphates (PIPs) through their PH domains, whereas the ligands of the rest of these proteins remain unclear (15). To determine the lipid specificity of evt-2 PH, we measured the binding of several negatively charged lipids on liposomes to recombinant evt-2 PH. Unexpectedly, PS bound to the PH, but phosphatidic acid, phosphatidylinositol, sulfatide, and all PIPs did not (Fig. 2 *A* and *B*). Lys20 is highly conserved in other PH domains (18). Evt-2 PH (K20E) lost the ability to bind to PS.

A *Saccharomyces cerevisiae* mutant (*cho1*Δ) deficient in PS (19, 20) is used to analyze protein binding to PS in vivo (4, 5). We expressed evt-2 PH in wild-type yeast and found that it was not associated with the PM. Because a tandem fusion of lipid-binding modules, such as the FYVE domain of EEA1 and Hrs, greatly enhances the lipid-binding affinity of the FYVE domain (21), we generated a tandem evt-2 PH (*2 × PH*) and expressed it in both the wild-type and *cho1*Δ mutant. *2 × PH* was observed predominantly on the PM of the wild-type yeast, whereas it was cytosolic in the PS-deficient mutant (Fig. 2*C*). The C2 domain of lactadherin (Lact-C2), a specific probe for PS (4), was used as a positive control. These findings showed that evt-2 PH recognizes PS in vivo.

Several intracellular organelles possess unique phospholipids such as PIPs, although the specific phospholipids in REs are not well characterized (22). We therefore expressed a variety of phospholipid probes in cells to see their distribution. None of the PIP probes stained REs (Fig. S5), but Lact-C2 predominantly stained REs and the PM (Fig. 2*D*, for quantification see Fig. S2*B*), revealing that REs are most enriched with PS among intracellular organelles. The enrichment of PS in REs was also confirmed in HeLa cells (Fig. S4*B*). Given the ligand specificity of the evt-2 PH, the binding of evt-2 PH to PS is likely to be involved in evt-2 localization to REs.

We were able to grow crystals of human evt-2 PH (a recombinant 110-amino acid domain) in complex with O-phospho-L-serine, the head group of PS, and analyzed them by X-ray crystallography at 1.0 Å resolution. The data collection and refinement statistics are summarized in Table S1. The overall structure was similar to the standard PH domain fold, with seven β strands forming two orthogonal antiparallel β sheets and two α helices containing the major C-terminal α helix (Fig. 3*A*). O-phospho-L-serine binds to the positively charged pocket made by three basic residues (Arg11, Arg18, and Lys20) and the backbone nitrogen atoms of three residues (Thr14, Ile15, and Leu16) of the β1/β2 loop (Fig. 3 *B* and *C* and Table S2). Arg11 and Arg18 each make two salt bridges with the L-serine oxygen atoms and the phosphate oxygen of the ligand, respectively (Fig. 3*B* and Table S2). In addition, Lys20 makes salt bridges with both moieties of the ligand. The nitrogen atom of O-phospho-L-serine forms a salt bridge with the side chain of Glu44 in one of the two conformers in the crystal (Fig. S6*A*).

We next examined whether the amino acid residues involved in the ligand binding in the crystal are essential for evt-2 localization to REs. The full-length point mutant *K20E*, in which Lys20 was changed to Glu, lost RE localization and showed puncta around the Golgi (Fig. 4*A*, for quantification see Fig. S2*A*). These puncta did not colocalize with TfnR (REs), but colocalized in part with VPS26 (EEs) and CD63 (late endosomes,LEs). The PH point mutant of Arg11, Arg18, or Lys20 (*PH(R11E)*, *PH(R18E)*, and *PH(K20E)*) did not show any specific membrane localization (Fig. 4*B*), suggesting that these residues bind to the head group of PS in vivo. All of the residues involved in the direct interaction of the ligand (Table S2) were conserved in the evt-2 PH of other species (Fig. 4*C*), further implicating these residues in the recognition of PS.

Two membrane trafficking pathways pass through REs: one is a recycling pathway and the other is a retrograde pathway that links the PM to the Golgi/ER (10). We examined whether evt-2 is involved in these pathways. Evt-2 knockdown did not cause any gross change in Tfn recycling to the PM (Fig. S7 *A* and *B*). Cholera toxin travels from the PM through endosomes (EEs/REs) to the Golgi/ER, and is finally translocated into the cytosol (11). Alexa 594-labeled cholera toxin B subunit (CTxB) was pulsed for 5 min and chased (Fig. 5*A*). After a 5-min uptake, CTxB accumulated around the Golgi, colocalizing in part with VPS26, showing that it reached EEs (Fig. S8*A*). After a 15-min pulse/chase, CTxB accumulated at the cell center, colocalizing with Tfn, showing it reached REs (Fig. S8*B*). After a 60–90 min pulse/chase, CTxB showed a good

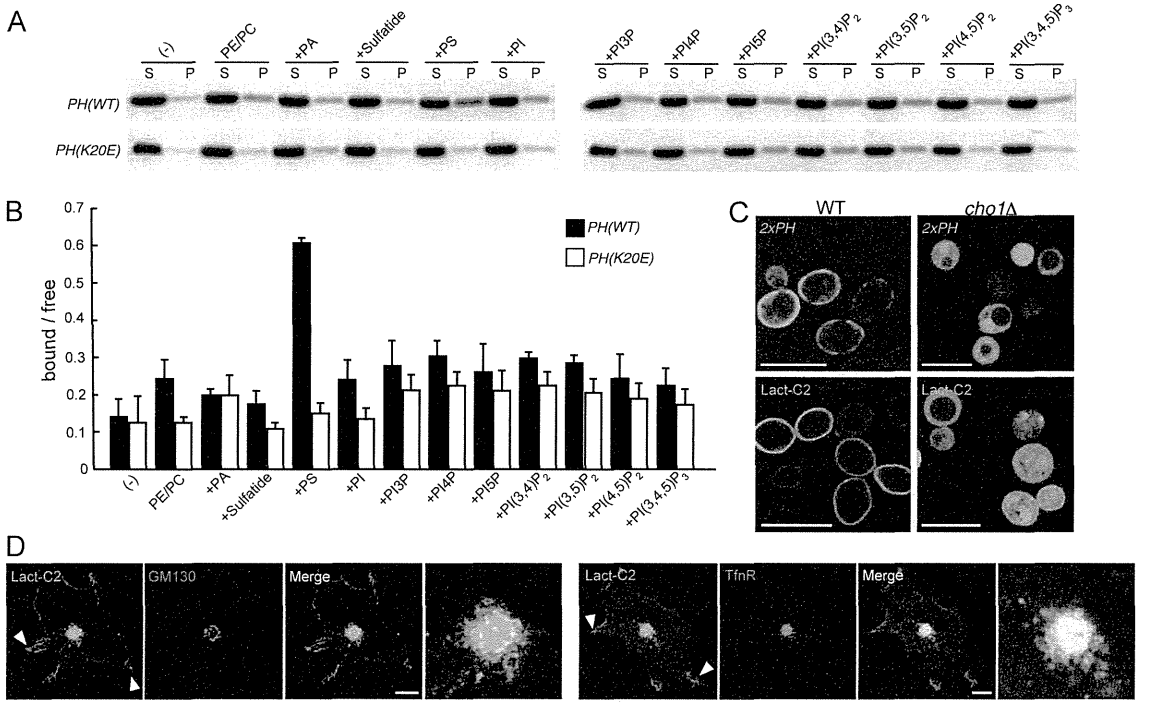

Fig. 2. Evt-2 PH binds to PS. (*A* and *B*) His-tagged evt-2 PH (WT or K20E) was mixed with liposomes harboring the indicated negatively charged lipid (20% mol/mol of total lipids). After 15 min, the mixture was spun at 100,000 *g* for 30 min, and the resultant supernatant (S) and pellet (P) were subjected to SDS-PAGE. The gels were stained with Coomassie blue (*A*). The intensities of individual bands were quantitated with NIH ImageJ. The values of "P (bound)/S (free)" are shown in a bar graph (*B*). Data represent mean values ± SD of three independent experiments. PE, phosphatidylethanolamine; PC, phosphatidylcholine; PA, phosphatidic acid; PI, phosphatidylinositol. (*C*) Confocal images of wild-type yeast cells and *cho1*Δ cells expressing GFP-tagged *2 × PH* (a tandem fusion of evt-2 PH) or GFP–Lact-C2. (Scale bars, 10 μm.) (*D*) COS-1 cells were transfected with GFP–Lact-C2, then fixed, and stained for GM130 or TfnR. Arrowheads indicate PM. (Scale bars, 10 μm.)

colocalization with GM130. These results showed the sequential retrograde transport of CTxB from the PM to the Golgi through EEs and then REs. In cells depleted of evt-2 by using siRNA 1 (Fig. 5*B*), CTxB transport to REs proceeded normally after a 15-min pulse/chase, but CTxB transport from REs to the Golgi was significantly impaired after a 60- or 90-min pulse/chase. The other siRNA oligos 2 and 3 also impaired CTxB traffic to the Golgi (Fig. S7*C*, for quantification see *D*). Thus, evt-2 is required for retrograde transport of CTxB from REs to the Golgi.

The effect of evt-2 knockdown on retrograde transport was also examined by biochemical assays using a mutant CTxB (CTxB-GS) harboring tyrosine sulfation and N-glycosylation sites to monitor its arrival at the Golgi or ER (23), and using cholera toxin to measure the increase of intracellular cAMP that occurs when the toxin

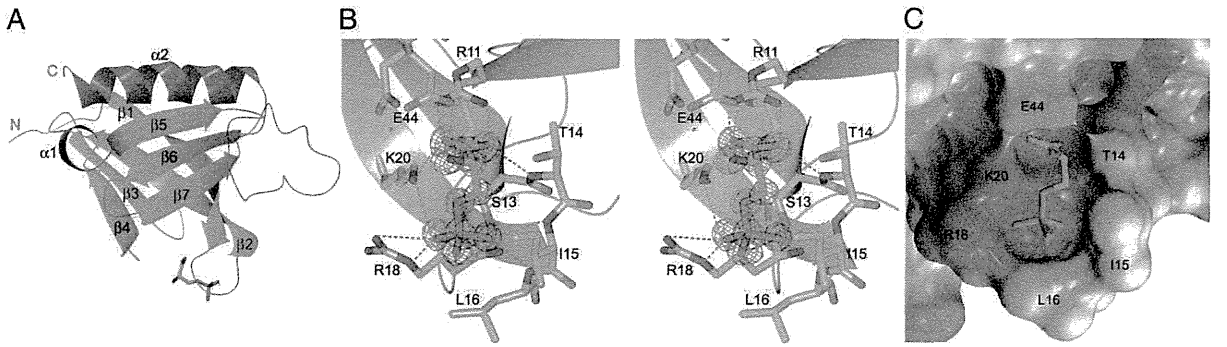

Fig. 3. High-resolution structure of evt-2 PH bound to phosphoserine. (*A*) Overall structure of human evt-2 PH in complex with O-phospho-L-serine, consisting of seven β strands and two helices. The amino and carboxy termini are denoted in red as N and C, respectively. O-phospho-L-serine is shown as a stick model. (*B*) Stereoview of the O-phospho-L-serine binding site of evt-2 PH. Interacting residues are shown as stick models. A σ_A-weighted *Fo-Fc* omit map (3.0 σ level; in gray mesh) is superposed on O-phospho-L-serine. Hydrogen bonds and salt bridges are shown as red broken lines. (*C*) Charge distribution surface model of evt-2 PH in complex with O-phospho-L-serine (stick model). The surface is colored according to the electrostatic potential of the residues (blue, positive; red, negative). Only one of the double conformers of Glu44 is shown.

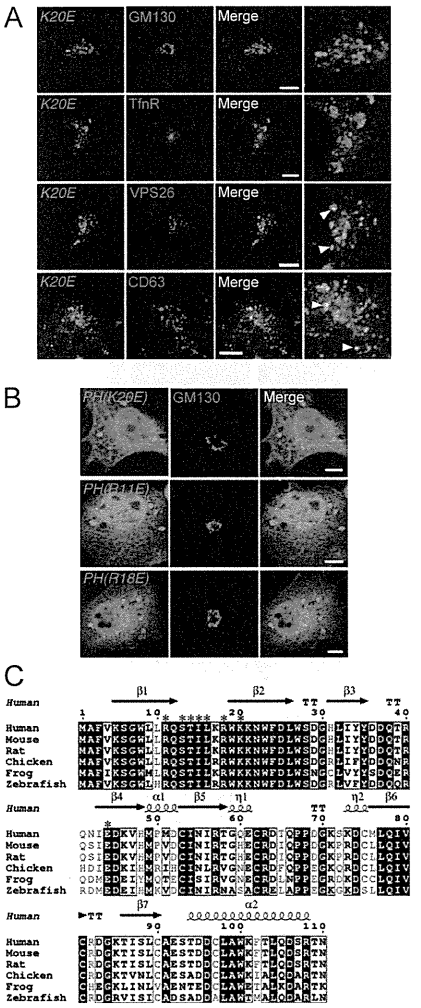

Fig. 4. The amino acid residues involved in the ligand binding in the crystal are essential for evt-2 localization to REs. (*A*) The full-length point mutant *K20E*, in which Lys20 was changed to Glu, was transiently expressed in COS-1 cells. The cells were then fixed and stained for Myc, GM130, TfnR, VPS26, and CD63. Arrowheads indicate puncta where *K20E* and endosomal markers are juxtaposed or colocalized. (Scale bars, 10 μm.) (*B*) The PH point mutants *PH (K20E)*, *PH(R11E)*, and *PH(R18E)*, in which Lys20, Arg11, or Arg18 was changed to Glu, were transiently expressed. The cells were then fixed and stained for Myc and GM130. (Scale bars, 10 μm.) (*C*) Alignment of vertebrate evt-2 PH domains. The secondary structure elements of human evt-2 PH are shown above the sequence. Conserved residues are boxed in white on a black background. Similar residues are boxed in black with a white background. Asterisks indicate the residues directly involved in the interaction of the ligand.

arrives in the cytosol. Both assays confirmed the impaired retrograde traffic of cholera toxin upon depletion of evt-2 (Fig. 5 *C* and *D* and Fig. S7*E*).

Evt-2 depletion did not significantly alter the subcellular localizations of a Golgi marker (GM130), a lysosomal marker (LAMP2), LE markers [CD63 and cation-independent mannose 6-phosphate receptor (CI-MPR)], or an RE marker (TfnR) (Fig. S7*F*). However, Golgi proteins TGN46 and GP73 no longer localized to the Golgi, but localized on punctate structures upon evt-2 depletion (Fig. 5*E*, for quantification see Fig. S2*C*). These two proteins are known to circulate between the Golgi and the PM through endosomes (10, 24). When retrograde transport from REs to the Golgi is impaired by depletion of evt-2, TGN46 and GP73 may be shunted to circulate among PM, EEs, and REs, resulting in their puncta localization.

Next, we performed knockdown/rescue experiments. Cells were depleted of evt-2 with siRNA 1 and transfected with an siRNA-resistant evt-2 construct (a mouse evt-2 WT or K20E mutant defective in PS binding). Golgi localization of TGN46 was restored in the cells transfected with mouse evt-2 WT (Fig. 5*F*). In contrast, TGN46 remained scattered throughout the cytosol in the cells transfected with evt-2 K20E mutant. Therefore, the binding of evt-2 PH to PS is essential for evt-2 function in endosomal membrane trafficking.

We further examined how blocking PS would affect endosomal membrane transport. Lact-C2 was overexpressed to mask PS in the cytosolic leaflet of REs. CTxB transport to the Golgi was severely delayed and accumulated in REs in the cells transfected with Lact-C2 (Fig. 5*G*, for quantification see Fig. S2*D*), showing that exposure of PS in the cytosolic surface of REs is required for CTxB transport from REs to the Golgi.

Recent studies in yeast and mammalian cells have established that the retromer complex at EEs has a critical function in retrograde membrane traffic to the Golgi (8, 25). In this study, besides EEs, we showed that REs are involved in this membrane traffic for certain cargo proteins. Retrograde and recycling traffickings diverge at REs, with a previously uncharacterized PH-domain–containing protein evt-2, which is essential and specific for retrograde traffic. We found that GP73, which circulates between the Golgi and the PM through endosomes, binds to evt-2 (Fig. S9). Together with the fact that evt-2 depletion abolished GP73 localization at the Golgi (Fig. 5*E*), we assume that evt-2 functions as a sorting device at REs to recruit specific cargo molecules that follow retrograde transport to the Golgi. We and other groups have shown that REs also play an obligatory role in the exocytic pathway for various secretory cargos (17, 26, 27). REs, therefore, can handle three membrane trafficking pathways: the recycling pathway (EEs → REs → PM), the exocytic pathway (the Golgi → REs → PM), and the retrograde pathway (EEs → REs → the Golgi).

The PH domain in evt-2 specifically binds PS, but not PIPs. What is the structural basis underlying the specificity of evt-2 PH to PS? All high-affinity, stereospecific PH domains for PIPs share a similar binding site (15). The β1/β2 loop functions as a platform for the interaction with the head group of the ligand. This loop lines a deep binding pocket and contains the sequence motif $KX_n(K/R)XR$ (where X is any amino acid), in which the basic side chains participate in most phosphate-group interactions. The corresponding motif in evt-2 PH is $R^{11}X_nK^{20}XN$, where italics indicate changes, and of note, the two nitrogen atoms (Nη1 and Nη2) of Arg11 make two salt bridges neatly with the carboxyl group of O-phospho-L-serine, which is absent in PIPs. A search for 3D structures homologous to human evt-2 PH using the DALI server (28) yielded the DAPP1/PHISH PH domain in complex with Ins(1,3,4,5)P_4 (Protein Data Bank code, 1FAO) as the best match (29). A comparison of the structures of the two complexes suggests that some evt-2 PH amino acids would clash with the head group of Ins(1,3,4,5)P_4 (Fig. S6 *B* and *C*). Thr14, Ile15, and Leu16 of evt-2 PH are close to the ligand, and the ligand-binding site is much smaller than that of DAPP1 PH. Therefore, the tightness of the ligand-binding site might account for the specificity of evt-2 PH for PS. Several simultaneous recognitions were identified in evt-2 PH (Fig. 3*B* and Table S2). Among them, Lys20 and Ile15 appear particularly important because they recognize both the L-serine and phosphate regions of the ligand. Simultaneous recognition of multiple regions of a ligand by interacting residues might enhance the binding affinity and specificity.

CELL BIOLOGY

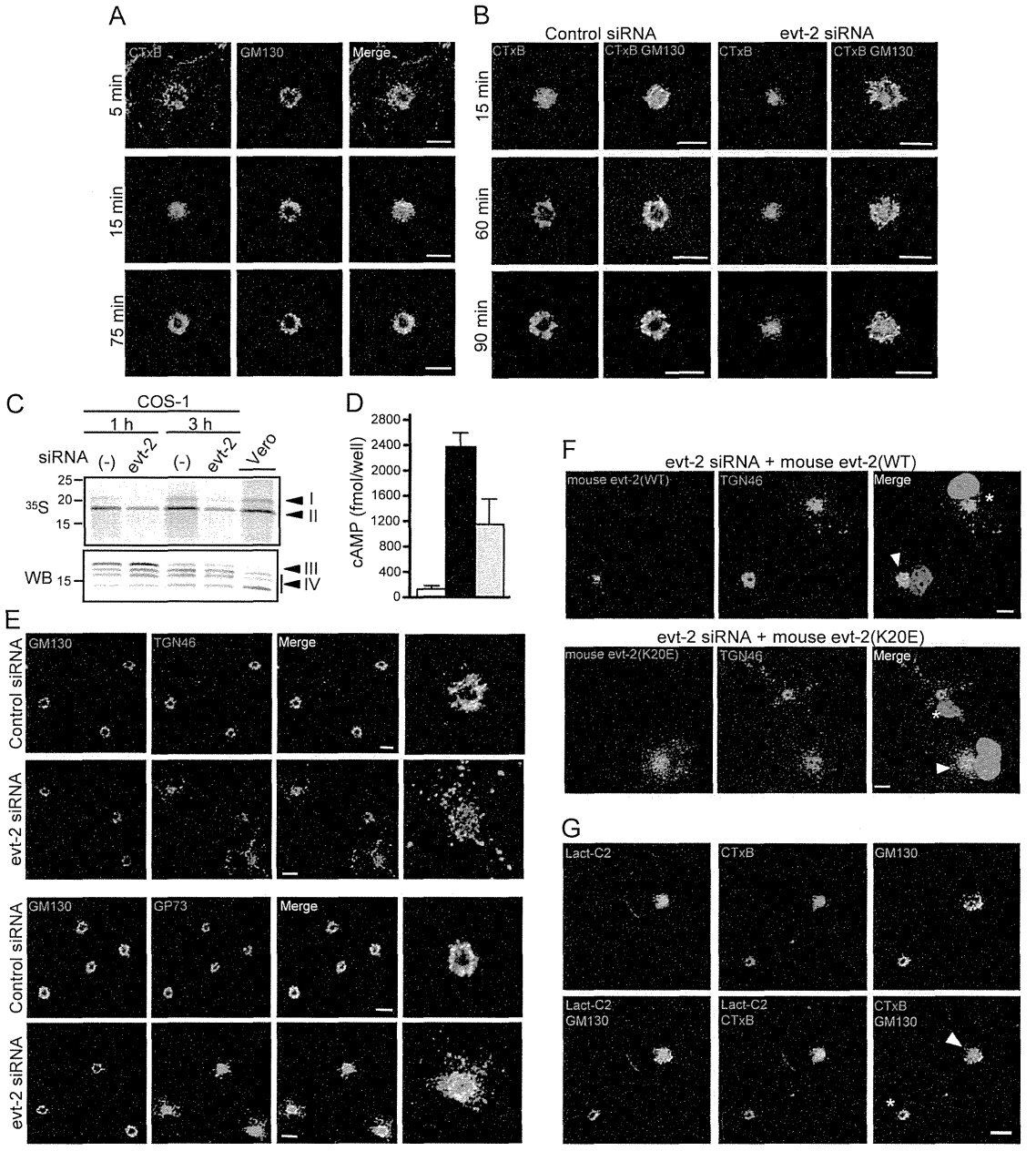

Fig. 5. Evt-2 and PS regulate retrograde transport through REs. (*A*) COS-1 cells were pulsed for 5 min at 37 °C with Alexa 594-CTxB and chased. Cells were then fixed at the indicated times from the beginning of the pulse, and stained for GM130. (Scale bars, 10 μm.) (*B*) Cells were treated with evt-2 siRNA 1 or control siRNA for 48 h. The pulse/chase of CTxB was performed as described in *A*. (Scale bars, 10 μm.) (*C*) Cells were treated with evt-2 siRNA 1 or mock treated for 48 h. Cells were then incubated with ^{35}S and CTxB-GS at 37 °C. CTxB-GS was immunoprecipitated and analyzed by autoradiography (*Upper*). A parallel experiment on Vero cells was carried out as control. The *Lower* band (II) represents the sulfated, but nonglycosylated CTxB. The *Upper* band (I) is N glycosylated. Thus, CTxB traveled from the PM to the Golgi and a significant fraction of the Golgi-modified protein moved to the ER. In cells depleted of evt-2, the intensity of ^{35}S-labeling of CTxB at both 1 and 3 h was reduced by 62–68%. In contrast, transport of CTxB beyond the Golgi to the ER was not affected (about 10% of the sulfated CTxB was glycosylated in both conditions). (*Lower*) Immunoblot (WB) of samples using an antibody against CTxB as loading control for autoradiogram. *Top* band (III) shows CTxB-GS. Bands labeled IV are degradation products. (*D*) Cells were treated with either evt-2 siRNA 1 or transfection reagent only for 48 h. Following addition of 1 nM cholera toxin, intracellular cAMP levels were measured at 50-min time point: evt-2 siRNA-treated cells (gray column), control cells (transfection reagent only, black column), and the cells without cholera toxin addition (white column). Data represent mean values of three independent experiments. (*E*) Cells treated with either evt-2 siRNA 1 or control siRNA were fixed and costained for GM130/TGN46 or GP73/GM130. Magnified images around the Golgi/REs region in one of the cells for each condition are shown in the *Right* column. (Scale bars, 10 μm.) (*F*) Cells were cotransfected with evt-2 siRNA 1 and siRNA-resistant mouse evt-2 constructs tagged with Myc (WT or K20E). After 72 h, cells were fixed and costained for Myc/TGN46. Arrowheads indicate cells expressing evt-2, and asterisks indicate nonexpressing cells. (Scale bars, 10 μm.) (*G*) Transient expression of GFP–Lact-C2. Cells were pulsed for 5 min with Alexa 594-CTxB, chased, fixed at 60 min after the beginning of the pulse, and stained for GM130. The arrowhead indicates a cell expressing GFP–Lact-C2, and the asterisk indicates a nonexpressing cell. (Scale bar, 10 μm.)

In this study, we showed that PS recognition by the PH domain of evt-2 is essential for endosomal membrane transport from the PM to the Golgi. The data presented here provide compelling evidence that intracellular PS has a critical role in membrane traffic and uncover the molecular basis that controls the RE-to-Golgi transport.

Materials and Methods

Cell Culture and Transfection. COS-1 cells were cultured at 37 °C with 5% CO_2 in DMEM containing 10% heat-inactivated FCS. Transfection was performed using Lipofectamine 2000 (Invitrogen) according to the manufacturer's instructions.

Structure Determination. The complex structure of human evt-2 PH with O-phospho-L-serine was determined by the molecular replacement method at 1.0 Å resolution using the data collected at beamline AR-NW12A of the Photon Factory. The crystal belongs to space group $P2_1$, with a = 31.7 Å, b = 48.4 Å, c = 64.3 Å, and β = 92.2°. The coordinates and structure factors of the human evt-2 PH structure have been deposited in the Protein Data Bank with the accession code 3AJ4.

Additional materials and methods are provided in *SI Materials and Methods*.

ACKNOWLEDGMENTS. A special thanks to Wendy Hamman for help with tissue culture and transfection conditions. This work was supported by the Core Research for Evolutional Science and Technology, Japan Science and Technology Agency (H.A. and T.T.), the Program for Promotion of Basic and Applied Research for Innovations in Bio-Oriented Industry (H.A.), the 21st Century Center of Excellence Program from the Ministry of Education, Culture, Sports, Science, and Technology of Japan (T.T.), Grants-in-aid for Scientific Research (20370045 to H.A. and 18050019 to T.T.), and a Senri Life Science Foundation Grant (to T.T.).

1. Leventis PA, Grinstein S (2010) The distribution and function of phosphatidylserine in cellular membranes. *Annu Rev Biophys* 39:407–427.
2. Huang M, et al. (2003) Structural basis of membrane binding by Gla domains of vitamin K-dependent proteins. *Nat Struct Biol* 10:751–756.
3. Verdaguer N, Corbalan-Garcia S, Ochoa WF, Fita I, Gómez-Fernández JC (1999) Ca(2+) bridges the C2 membrane-binding domain of protein kinase Calpha directly to phosphatidylserine. *EMBO J* 18:6329–6338.
4. Yeung T, et al. (2008) Membrane phosphatidylserine regulates surface charge and protein localization. *Science* 319:210–213.
5. Moravcevic K, et al. (2010) Kinase associated-1 domains drive MARK/PAR1 kinases to membrane targets by binding acidic phospholipids. *Cell* 143:966–977.
6. Gagescu R, et al. (2000) The recycling endosome of Madin-Darby canine kidney cells is a mildly acidic compartment rich in raft components. *Mol Biol Cell* 11:2775–2791.
7. Mellman I, Warren G (2000) The road taken: Past and future foundations of membrane traffic. *Cell* 100:99–112.
8. Bonifacino JS, Rojas R (2006) Retrograde transport from endosomes to the trans-Golgi network. *Nat Rev Mol Cell Biol* 7:568–579.
9. Johannes L, Popoff V (2008) Tracing the retrograde route in protein trafficking. *Cell* 135:1175–1187.
10. Maxfield FR, McGraw TE (2004) Endocytic recycling. *Nat Rev Mol Cell Biol* 5:121–132.
11. Lencer WI, Tsai B (2003) The intracellular voyage of cholera toxin: Going retro. *Trends Biochem Sci* 28:639–645.
12. Sandvig K, van Deurs B (2002) Membrane traffic exploited by protein toxins. *Annu Rev Cell Dev Biol* 18:1–24.
13. Mallard F, et al. (1998) Direct pathway from early/recycling endosomes to the Golgi apparatus revealed through the study of shiga toxin B-fragment transport. *J Cell Biol* 143:973–990.
14. Krappa R, Nguyen A, Burrola P, Deretic D, Lemke G (1999) Evectins: Vesicular proteins that carry a pleckstrin homology domain and localize to post-Golgi membranes. *Proc Natl Acad Sci USA* 96:4633–4638.
15. Lemmon MA (2008) Membrane recognition by phospholipid-binding domains. *Nat Rev Mol Cell Biol* 9:99–111.
16. Misaki R, Nakagawa T, Fukuda M, Taniguchi N, Taguchi T (2007) Spatial segregation of degradation- and recycling-trafficking pathways in COS-1 cells. *Biochem Biophys Res Commun* 360:580–585.
17. Misaki R, et al. (2010) Palmitoylated Ras proteins traffic through recycling endosomes to the plasma membrane during exocytosis. *J Cell Biol* 191:23–29.
18. Dowler S, et al. (2000) Identification of pleckstrin-homology-domain-containing proteins with novel phosphoinositide-binding specificities. *Biochem J* 351:19–31.
19. Atkinson KD, et al. (1980) Yeast mutants auxotrophic for choline or ethanolamine. *J Bacteriol* 141:558–564.
20. Hikiji T, Miura K, Kiyono K, Shibuya I, Ohta A (1988) Disruption of the CHO1 gene encoding phosphatidylserine synthase in Saccharomyces cerevisiae. *J Biochem* 104: 894–900.
21. Gillooly DJ, et al. (2000) Localization of phosphatidylinositol 3-phosphate in yeast and mammalian cells. *EMBO J* 19:4577–4588.
22. Di Paolo G, De Camilli P (2006) Phosphoinositides in cell regulation and membrane dynamics. *Nature* 443:651–657.
23. Fujinaga Y, et al. (2003) Gangliosides that associate with lipid rafts mediate transport of cholera and related toxins from the plasma membrane to endoplasmic reticulm. *Mol Biol Cell* 14:4783–4793.
24. Puri S, Bachert C, Fimmel CJ, Linstedt AD (2002) Cycling of early Golgi proteins via the cell surface and endosomes upon lumenal pH disruption. *Traffic* 3:641–653.
25. Seaman MN, McCaffery JM, Emr SD (1998) A membrane coat complex essential for endosome-to-Golgi retrograde transport in yeast. *J Cell Biol* 142:665–681.
26. Ang AL, et al. (2004) Recycling endosomes can serve as intermediates during transport from the Golgi to the plasma membrane of MDCK cells. *J Cell Biol* 167:531–543.
27. Murray RZ, Kay JG, Sangermani DG, Stow JL (2005) A role for the phagosome in cytokine secretion. *Science* 310:1492–1495.
28. Holm L, Sander C (1995) Dali: A network tool for protein structure comparison. *Trends Biochem Sci* 20:478–480.
29. Ferguson KM, et al. (2000) Structural basis for discrimination of 3-phosphoinositides by pleckstrin homology domains. *Mol Cell* 6:373–384.

Angiopoietin-Like 2, a Circadian Gene, Improves Type 2 Diabetes Through Potentiation of Insulin Sensitivity in Mice Adipocytes

Masashi Kitazawa, Mamoru Nagano, Koh-hei Masumoto, Yasufumi Shigeyoshi, Tohru Natsume, and Seiichi Hashimoto

Biomedicinal Information Research Center, National Institute of Advanced Industrial Science and Technology (M.K., T.N.) and Japan Biological Informatics Consortium (M.K.), Tokyo 135-0064, Japan; Department of Anatomy and Neurobiology (M.N., K.-h.M., Y.S.), Kinki University School of Medicine, Osaka 589-8511, Japan; Laboratory for Systems Biology (K.M.), RIKEN Center for Developmental Biology, Hyogo 650-0047, Japan; and Graduate School of Medicine (S.H.), University of Tokyo, 7–3-1 Hongo, Bunkyo, Tokyo 113-0033, Japan

Angiopoietin-like (Angptl)2, a member of the Angptl protein family, is predominantly secreted from adipose tissue and the heart. Here, we demonstrate that the expression of Angptl2 in epididymal adipose tissue of C57BL/6J mice shows pulsatility and circadian rhythmicity and that the rhythmicity was disrupted in high-fat-fed and leptin receptor-deficient diabetic db/db mice with insulin resistance. To investigate whether the reduction in Angptl2 expression was related to the progression of diabetes, we treated db/db mice with recombinant Angptl2 for 4 wk during the peak period of Angptl2 expression in C57BL/6J mice. Angptl2-treated mice showed decreases in plasma glucose, insulin, triglyceride, and fatty acid levels and an increase in plasma adiponectin, a therapeutic regulator of insulin resistance, leading to improvements in glucose tolerance. In cultured adipocytes, recombinant Angptl2 increased adiponectin expression and stimulated insulin sensitivity partially by reducing the levels of tribbles homolog 3, a specific Akt kinase inhibitory protein. Conversely, Angptl2 small interfering RNA reduced adiponectin expression, resulting in insulin resistance. In preadipocytes, treatment with Angptl2 small interfering RNA inhibited differentiation to adipocytes and reduced adiponectin expression. Taken together, our results suggest that replenishment of Angptl2 stimulates insulin sensitivity and improves the type 2 diabetic state. (***Endocrinology*** **152: 2558–2567, 2011)**

Angiopoietin-like (Angptl) proteins have been identified as several molecules containing a coiled-coil domain and a fibrinogen-like domain, motifs that are structurally conserved in angiopoietins. However, none of these proteins bind to either tyrosine kinase with immunoglobulin-like and EGF-like domains 2 or 1 and are still considered orphan ligands. Several studies have shown that Angptl have the potential to regulate angiogenesis by their action as angiopoietins. In addition, some Angptl are potent regulators of lipid, glucose, and energy metabolism. For example, Angptl3 and Angptl4 regulate triglyceride metabolism by suppressing lipoprotein lipase (1, 2). There is also evidence that Angptl6/angiopoietin-related growth factor (AGF)-deficient mice have significantly larger both visceral and sc fat depots than wild-type mice (3). Furthermore, AGF suppresses gluconeogenesis in hepatocytes (4). On the basis of these findings, it appears that Angptl plays a role in the regulation of metabolic function.

Energy homeostasis, including glucose and lipid metabolism, is subject to circadian regulation that synchronizes energy intake and expenditure with changes in the external environment throughout the daily 24-h cycle (5). Circadian clocks are present in most tissues of the body,

ISSN Print 0013-7227 ISSN Online 1945-7170
Printed in U.S.A.

doi: 10.1210/en.2010-1407 Received December 7, 2010. Accepted April 26, 2011.
First Published Online May 17, 2011

Abbreviations: AGF, Angiopoietin-related growth factor; Angptl, angiopoietin like; AS160, Akt substrate of 160 kDa; CD68, cluster of differentiation 68; FoxO1, forkhead box protein O1; IRS, insulin receptor substrate; LD, 12-h light, 12-h dark cycle; PPAR, peroxisome proliferator-activated receptor; SDS, sodium dodecyl sulfate; siRNA, small interfering RNA; Trib3, tribbles homolog 3; ZT, Zeitgeber time.

where they control the expression of 5–10% of tissue-specific mRNA through both transcriptional and post-transcriptional regulation (6, 7). The central clock gene Clock:Bmal1 dimerizes to drive the expression of circadian effector genes implicated in a multitude of physiological functions (8, 9). Mutations in the central clock genes, Clock and Bmal1, result in metabolic changes leading to obesity and the metabolic syndrome (10–12). Kohsaka *et al.* (13) demonstrated recently that a high-fat diet disrupts the expression of circadian clock-controlled genes involved in fuel utilization in the liver and adipose tissue. These reports suggest that circadian genes play a crucial role in obesity and the metabolic syndrome.

In this study, we sought to identify the circadian genes in the Angptl family and found that both Angptl2 and Angptl4 act as circadian genes in adipose tissue (Supplemental Fig. 1, published on The Endocrine Society's Journals Online web site at http://endo.endojournals.org). Several studies have reported that Angptl2 induces sprouting in endothelial cells (14, 15), indicating a role in angiogenesis. Based on amino acid similarity, Angptl2 is notably closer to the antidiabetic factor Angptl6/AGF than it is to Angptl3 or Angptl4, factors which accelerate hyperglycemia (16). From these reports, we speculated that Angptl2 is an antidiabetic factor. To verify this assumption, we investigated whether administration of Angptl2 improved changes associated with diabetes in db/db mice. We also demonstrated that Angptl2 enhanced insulin sensitivity in adipocytes.

Materials and Methods

Animals

All experiments were conducted using 12-wk-old male mice. We obtained 5-wk-old C57BL6J mice and diabetic db/db mice from Charles River Laboratories (Germantown, MD). The mice were maintained on a 12-h light, 12-h dark cycle (LD) in normal cages with food and water *ad libitum*. Zeitgeber time (ZT) was used as the time scale for the LD conditions. ZT0 represents lights on and ZT12 represents lights off. For high-fat feeding, mice were fed D12451 (45% of kilocalories from fat; Research Diets, Inc., New Brunswick, NJ) for 7 wk. To investigate the antidiabetic effect of Angptl2, 8-wk-old db/db mice were injected ip with 0.8 mg/kg body weight Angptl2 at ZT12 for 4 wk. Tissue and serum samples were collected 2 h after the final administration of Angptl2. All experimental procedures were conducted according to the policies of the Animal Ethical Committee of Astellas Pharma, Inc. (Ibaraki, Japan).

Antibodies

The antibodies that recognize Angptl2 were from R&D Systems (Minneapolis, MN); the antiactin antibody was from Santa Cruz Biotechnology, Inc. (Santa Cruz, CA); the antibodies that recognize phosphorylated Thr308 and Ser473 on Akt, phosphorylated Thr202/Tyr204 on Erk1/2, phosphorylated Ser256 on forkhead box protein O1 (FoxO1), phosphorylated Ser636/639 on insulin receptor substrate (IRS)-1, anti-Akt, anti-Erk1/2, anti-FoxO1, and IRS-1 were from Cell Signaling Technology (Beverly, MA); the antibody that recognizes phosphorylated Thr642 on Akt substrate of 160 kDa (AS160) and anti-AS160 were from Upstate (Waltham, MA); and the antibody that recognizes tribbles homolog 3 (Trib3) was from Calbiochem (La Jolla, CA).

Circadian gene experiments

To investigate the circadian expression of genes, we collected epididymal adipose tissue and serum every 4 h over the course of 2 d under LD conditions. We began to sample epididymal adipose tissues at ZT0. Total RNA was prepared using Trizol reagent (Invitrogen/Life Technologies, Inc., Carlsbad, CA). Tissues lysates for Western blotting were prepared using sodium dodecyl sulfate (SDS) sampling buffer [1 mM EDTA, 1% SDS, and 10 mM HEPES-HCl (pH 7.5)] containing Complete (Roche Applied Science, Mannheim, Germany) and Phosphatase inhibitor cocktails (Sigma Chemical Co., St. Louis, MO). Albumin was removed from the serum samples using the ProteoExtract Albumin/IgG Removal kit (Calbiochem).

Quantitative PCR

Quantitative PCR was performed using SYBR Green Reagent on an ABI Prism 7700 machine (Applied Biosystems, Foster City, CA) as described previously (4). The oligonucleotides used for PCR are listed in Table 1.

Preparation of recombinant human Angptl2 protein

Purification of recombinant human Angptl2 protein was carried out as described by Ito and co-workers (15). Briefly, the conditioned medium from transfected HEK293 cells was collected and passed through a 0.22-μm pore size filter (Millipore, Bedford, MA). To purify Angptl2 protein, the filtered conditioned medium was transferred to an anti-FLAG antibody (M2) affinity gel (Sigma Chemical Co.), with only Angptl2 protein being trapped in the gel. After the gel was washed with PBS, the protein was eluted by adding Gly-HCl (pH 3.0) and immediately neutralized with Tris-HCl (pH 8.0). Angptl2 protein was dialyzed in PBS overnight at 4 C. Protein concentration was measured using the BCA protein assay kit (Pierce, Rockford, MA).

Metabolic measurements

Enzymatic assay kits were used to determine the levels of triglycerides (Sigma Chemical Co.) and nonesterified fatty acids (Roche Applied Science). Plasma glucose was measured by an Amplex Red Glucose/Glucose Oxidase Assay kit (Invitrogen, Carlsbad, CA) based on the immobilized glucose oxidase membrane/hydrogen peroxide electrode method. Plasma insulin was determined using a mouse insulin ELISA kit (Morinaga Biochemistry Co., Kanagawa, Japan) and plasma adiponectin by an ELISA kit (Otsuka Pharmaceutical Co., Tokushima, Japan).

Glucose tolerance test

Mice were fasted for 16 h and then injected ip with glucose (2 g/kg body weight) for measurement of plasma glucose at the indicated times.

TABLE 1. Quantitative PCR primers

Gene	Accession no.	Forward primer	Reverse primer
Angptl2	NM_011923	TGCCATTTGTGTCAACTCCAA	CACGATGCCTCCGTCTACCT
Angptl4	NM_020581	GCCAAATTGCTCCAATTTCCT	CGTGGTCTTGGTCCCAGGTA
G6pc	NM_008061	CAGGGCTGTTTGAGGAAAGTG	GGAAGATTCTGCACCGCAAG
Pck1	NM_011044	AGCATGCGCTGAGATCTAGGA	GGTGATTTCCCCTCCCAATC
Cpt1a	NM_013495	AGCGATGCAGAATCTCATTGG	GGGTCTCACTCTCCTTGCCA
Cyp7a1	NM_007824	TGATGTAACGACTGCTGAGCG	AAGTGATGAAACTCAGGCCCC
Acly	NM_134037	GGCTGGGACCATTGTATCCTT	GTCGGCTGCATGAACACAGA
Acacb	NM_133904	TACAGGTGGCTCAGCTGCTG	TGGAGTGGCTCCGTGAGTTT
Fasn	NM_007988	AGTGTTGGTGCAAGCCCTCT	CAAGCAACCTCCACTCCTCTG
Lpl	NM_008509	GAACACCAACCCACATGCAA	AGGCACAACCAGCTTTCTCCT
Il1b	NM_008361	GGCTGGACTGTTTCTAATGCCT	TTTGAACAGAATGTGCCATGGT
Il6	NM_031168	CTGGAGTCACAGAAGGAGTGGC	CCACAGTGAGGAATGTCCACAA
TNF-α	NM_013693	GATTATGGCTCAGGGTCCAACT	CATTCGAGGCTCCAGTGAATTC
MCP−1	NM_011333	CATCTGCCCTAAGGTCTTCAGC	GCATCACAGTCCGAGTCACACT
CD68	NM_009853	CCCAAGGAACAGAGGAAGACTG	GTGTGAACTGTGACATTTCCGTG
aP2	NM_024406	GCCAAGCCCAACATGATCA	ATTCCACGCCCAGTTTGAAG
Adipoq	NM_009605	CTGGCAGGAAAGGAGAGCCT	CCAGTGCTGCCGTCATAATG
Cebpa	NM_007678	CAAAGCCAAGAAGTCGGTGGAC	GCGGTCATTGTCACTGGTCAAC
Cebpb	NM_009883	AATCACCTTAAAGATGTTCCTGCG	TCGAAACGGAAAAGGTTCTCAA
Ppara	NM_011144	AATTAACGGGTAACCTCGAAGTCTG	TAAATGGCTAACCTTGGGCCAC
PParg	NM_011146	GCAGCTACTGCATGTGATCAAGA	GGGTGGGACTTTCCTGCTAATAC
Trib3	NM_175093	GCTGGCAGATACCCATTCCA	CCACAAGTCGCTCTGAAGGTTC
b-actin	NM_007393	TGAGAGGGAAATCGTGCGTGAC	AAGAAGGAAGGCTGGAAAAGAG

Cell culture

Mouse preadipocyte 3T3-L1 cells were grown and maintained in DMEM supplemented with 10% fetal bovine serum. For adipocyte differentiation, the cells were grown to full confluence for 2 d and then induced with differentiation medium containing 10 μg/ml insulin, 1 μM dexamethasone, and 0.5 mM isobutylmethylxanthine. After 2 d of induction, the cells were cultured for 2 d in progression medium containing 10 μg/ml insulin. The medium was then changed to DMEM with 10% fetal bovine serum for differentiation at 37 C and an atmosphere containing 5% CO_2.

Transfection

Angptl2 small interfering RNA (siRNA) and negative control siRNA were purchased from Invitrogen. Several siRNA oligonucleotides were screened and tested for their ability to inhibit Angptl2 expression. The most active of these oligonucleotides for mouse Angptl2 (sense, 5′-UGAAAGUGUAGGUGCACUUGUCGGG-3′; antisense, 5′-CCCGACAAGUGCACCUACACUUUCA-3′), mouse Trib3 (sense, 5′-CACAGUUGCUGAAGACAAAGCGACG-3′; antisense, 5′-CGUCGCUUUGUCUUCAGCAACUGUG-3′) effectively blocked the expression of Angptl2 or Trib3. We transfected 3T3-L1 preadipocytes and adipocytes with each of the siRNA at a final concentration of 30 nM using Lipofectamine RNAiMAX (Invitrogen). All the experiments were performed 2 d after transfection.

Glucose uptake assay

Day 7–11 3T3-L1 adipocytes were incubated for 3 h in serum- and glucose-free media. Basal and insulin-induced glucose uptakes were measured by rinsing the cells and then incubating in serum- and glucose-free media for 30 min with or without 1 nM insulin, followed by the addition of unlabeled 2-deoxy-D-glucose (1 mM) and 1 μCi of 2-deoxy-D-[^{14}C] glucose (Amersham Biosciencess/GE Healthcare, Princeton, NJ). After incubation for 5 min at room temperature, the media were removed, and the cells were washed in cold PBS and lysed in 300 μl of 0.1% SDS. The radioactivity associated with 50 μl was determined by liquid scintillation counting. The results were corrected for nonspecific binding using control cells incubated in the presence of 20 μM cytochalasin B. Glucose uptake was normalized to protein content as measured from the remaining cell lysates with BCA protein assay kit (Pierce).

Results

Disruption of rhythmic expression of Angptl2 in db/db and DIO mice

To determine whether mRNA expression of Angptl in epididymal adipose tissue showed daily rhythms, fat samples were obtained from 12-wk-old C57BL/6J mice every 4 h throughout a 48-h period. As shown in Fig. 1A, expression of the Angptl2 and Angptl4 genes exhibited 24-h rhythmicity. In addition, peak expression of Angptl2 mRNA at ZT12 corresponded with the peak period of food consumption and was opposite to the phase of Angptl4 mRNA expression, which peaked at ZT0. The rhythmic expression of Angptl2 mRNA (Fig. 1B) and protein (Fig. 1C) was disrupted in the epididymal fat of db/db mice as a result of reduced mRNA expression during the peak period. Angptl2 was expressed not only in fat but also in heart (Supplemental Fig. 2), although the reduction in Angptl2 mRNA was not observed in the heart at ZT12 (Fig. 1D). Serum Angptl2 levels were also found to show circadian expression and were reduced in db/db mice from

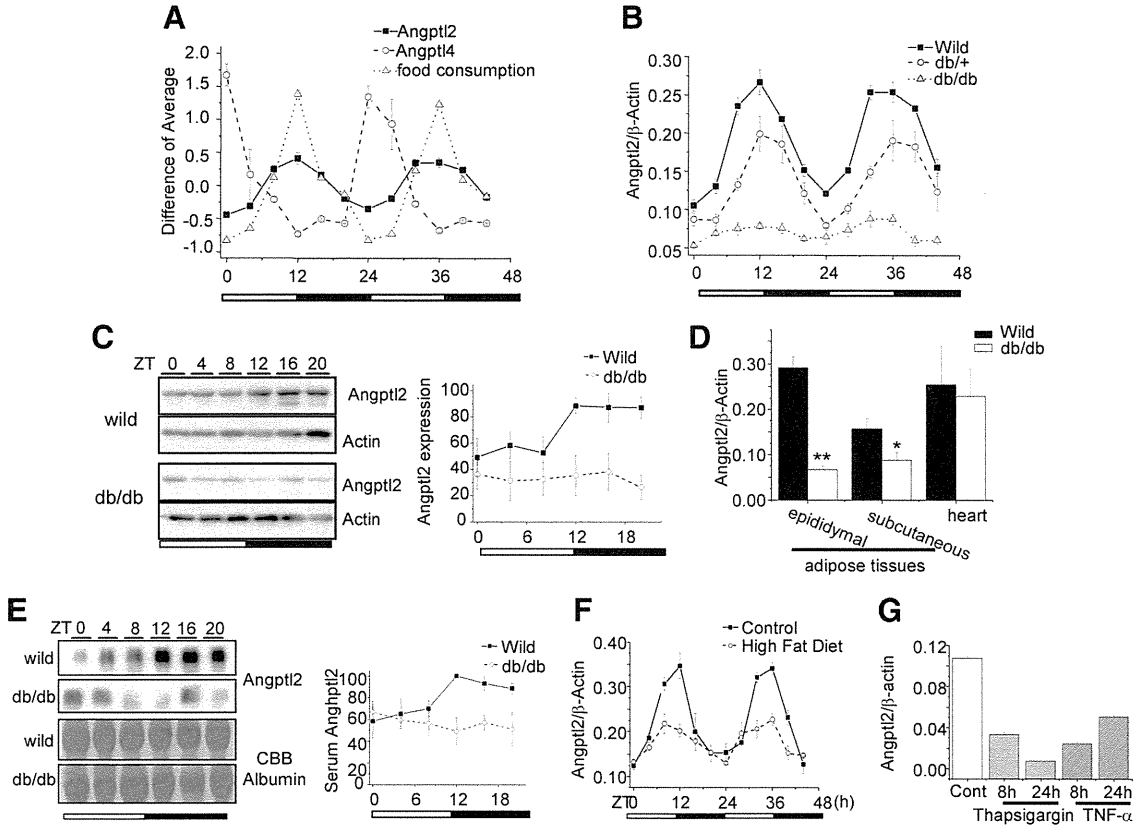

FIG. 1. Disruption of circadian expression of Angptl2 by diabetes and obesity in epididymal adipose tissue. A, Temporal expression profiles of Angptl2 and Angptl4 mRNA in epididymal adipose tissue from C57BL6 mice, determined by quantitative PCR assay (n = 3). Temporal pattern of food intake was calculated at every 4 h. In this and all other figures, the *error bars* represent ±SEM. Male mice aged 12 wk were used in the experiments. Data were normalized so that the average signal intensity of 24 time points was 0. B and C, Temporal expression profiles of Angptl2 mRNA (n = 3) (B) and protein (C) for each genotype. C, Immunoblotting was performed with anti-Angptl2 antibody. Actin was used as an internal control (*left panel*). The graph represents the ratio of band densities, comparing with maximum points (*right panel*) (n = 3). D, Angptl2 mRNA expression in epididymal and sc adipose tissues and heart of wild or db/db mice (n = 3). E, Temporal expression profiles of Angptl2 in serum. Representative Western blottings (*left panel*) and quantitative data (right *panel*) (n = 3) for the Angptl2 are shown. Coomassie Brilliant Blue-stained albumin is as control bands for protein loading. F, Temporal expression profiles of Angptl2 in epididymal adipose tissue of mice fed either a normal (CE-2) or high-fat diet (D12451) for 8 wk (n = 3). G, Angptl2 mRNA expression in differentiated 3T3-L1 adipocytes treated with 2 μM Thapsigargin or 10 ng/ml TNF-α for indicated time (n = 3). **, $P < 0.01$; *, $P < 0.05$ compared with wild mice.

ZT12 to ZT16 (Fig. 1E). Furthermore, the reduced expression of Angptl2 mRNA was also observed at ZT12 in mice with high-fat diet-induced obesity (Fig. 1F). Investigation of the relationship between Angptl2 expression and the major pathoetiology of diabetes showed that Angptl2 mRNA expression in differentiated 3T3-L1 adipocytes was reduced by 8- or 24-h treatment with either 2 μM thapsigargin, an endoplasmic reticulum stress inducer or 10 ng/ml TNF-α, major factor of insulin resistance (Fig. 1G).

Angptl2 improves circulating plasma glucose and lipid levels

To examine the effectiveness of Angptl2 in treating diabetes, db/db mice were administered a daily ip injection of recombinant human Angptl2 at 0.8 mg/kg body weight per day at ZT12 for 4 wk. The control group was treated with vehicle buffer (PBS) for the same interval. The plasma human Angptl2 concentration was approximately 100 ng/ml at 2 h after administration and decreased to less than 50 ng/ml at 12 h (Supplemental Fig. 3). These concentrations are similar to the active concentrations *in vitro* (15). These results also indicated that the administration of Angptl2 caused variations in its plasma concentration over time, as well as the physiological condition. No significant difference in daily food intake (PBS, 5.79 ± 0.188 g/d; Angptl2, 5.80 ± 0.139 g/d) or body weight was observed between the two groups (Fig. 2A). Epididymal adipose tissue weight was slightly decreased (PBS, 2.00 ± 0.117 g; Angptl2, 1.77 ± 0.092 g). A significant decrease in random-fed glucose levels was observed in the 2 wk after administration of Angptl2 compared with controls (Fig. 2A). The Angptl2-treated db/db mice also showed a decrease in serum insulin levels and increases in serum adiponectin levels and mRNA expression in mesenteric adipose tissues to levels similar to those in wild-type mice (Fig. 2B). An ip glucose tolerance test showed that db/db

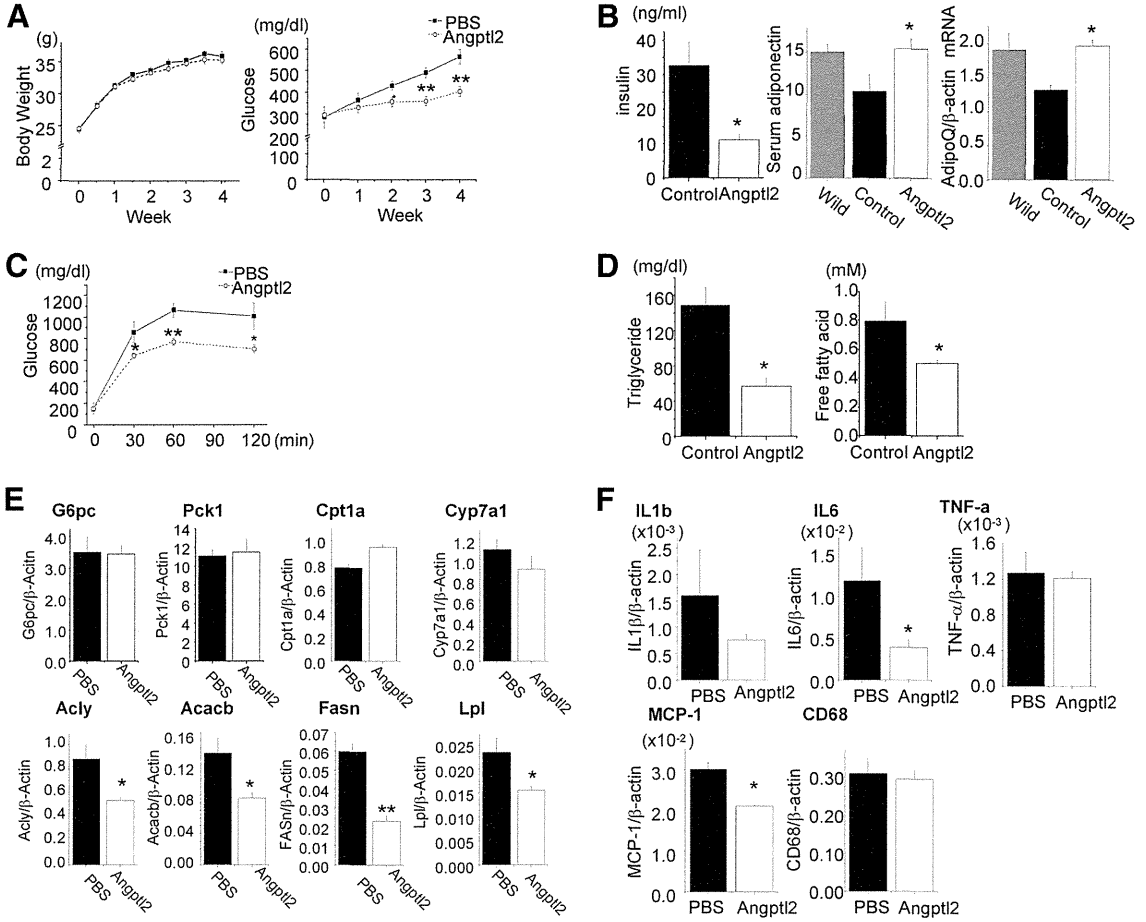

FIG. 2. Effects of Angptl2 on insulin resistance. Angptl2 or PBS control was administered to db/db mice for 4 wk. A, Body weight and fed blood glucose levels of db/db mice administered 0.8 mg/kg body weight per day Angptl2 or PBS at ZT12 for the indicated periods starting at 6 wk of age. B, Plasma insulin (*left*) and adiponectin (*middle*) concentrations and expression of adiponectin in mesenteric adipose tissues (*right*) in wild mice and db/db mice administered Angptl2 or PBS. C, Blood glucose concentrations during ip glucose tolerance tests in db/db mice administered Angptl2 or PBS for 4 wk. The final administration of Angptl2 was conducted at the start of fasting. Mice were fasted for 16 h and then injected ip with glucose (2 g/kg body weight). D, Serum triglyceride and free fatty acid concentrations in db/db mice administered Angptl2 or PBS. E, Quantitative RT-PCR of mRNA encoding fatty acid metabolism-, gluconeogenesis-, and cholesterol metabolism-related genes in liver. F, Quantitative RT-PCR of mRNA encoding inflammatory factors and macrophage markers in mesenteric adipose tissue (n = 5 animals per group). **, $P < 0.01$; *, $P < 0.05$ compared with vehicle control.

mice had improved glucose tolerance after Angptl2 treatment (Fig. 2C). Furthermore, serum triglyceride and free fatty acid levels also decreased with Angptl2 administration (Fig. 2D). We investigated mRNA expression in the liver of genes related to fatty acid synthesis (Acly, Acacb, Fasn, and Lpl) and oxidation (Cpt1a), gluconeogenesis (G6pc and Pck1), and cholesterol metabolism (Cyp7a1) (Fig. 2E). The expression of gluconeogenesis-related and cholesterol metabolism-related genes did not change significantly, whereas the expression of fatty acid synthesis and metabolism-related genes (Acly, Acacb, Fasn, and Lpl) was reduced in the liver of mice administered Angptl2. Inflammations in adipose tissues cause insulin resistance. We next examined the expression of mRNA for inflammatory cytokines (IL-1β, IL-6, and TNF-α), a chemokine (monocyte chemotactic protein-1), and macrophage marker [cluster of differentiation 68 (CD68)] in mesenteric adipose tissue. Administration of Angptl2 induced decreases in IL-6 and monocyte chemotactic protein-1 mRNA expression, whereas the expression of IL-1β, TNF-α, and CD68 remained unchanged (Fig. 2F).

Angptl2 is a regulator of adipogenesis in 3T3-L1 cells

We next investigated the effects of Angptl2 on premature and mature adipocytes using 3T3-L1 cells. Consistent with previous work that has shown mice treated with Angptl2 have increased serum adiponectin levels, expression of the adipocyte-specific protein, Angptl2 was highest in preadipocytes and in fully mature adipocytes, on d 0 and 7 of adipocyte differentiation (Fig. 3A). Based on this finding, we hypothesized that Angptl2 regulates adipocyte differentiation in an autocrine or paracrine manner. To test this hypothesis, we transfected confluent preadipocytes with Angptl2 siRNA or a negative control siRNA. Angptl2 siRNA reduced the expression levels of mRNA and

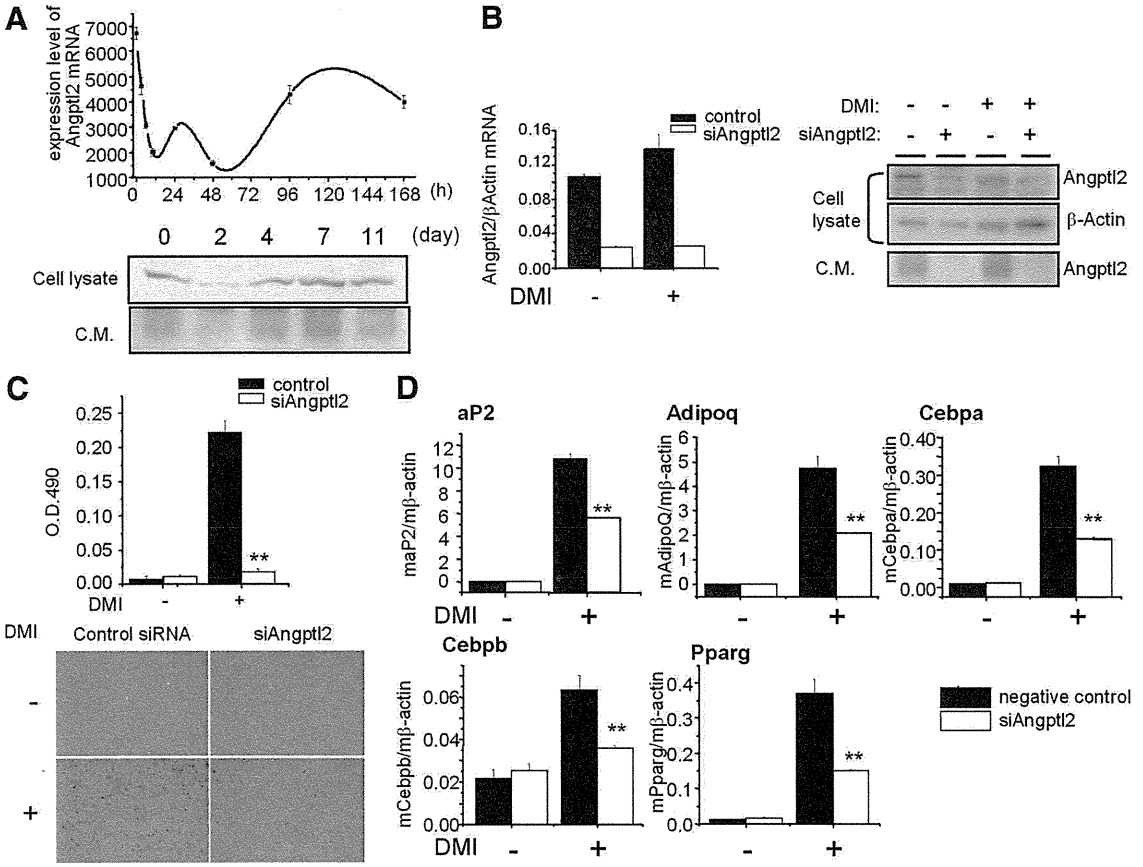

FIG. 3. Effects of Angptl2 on 3T3-L1 preadipocyte differentiation. A, Levels of Angptl2 mRNA (*upper panel*) and protein in the cell lysates or culture medium (*lower panel*) during differentiation of 3T3-L1 cells by dexamethasone, isobutylmethylxanthine and insulin (DMI). B, Effects of Angptl2 siRNA on mRNA (*left panel*) and protein (*right panel*) expression or secretion. Two days after siRNA transfection, cells were induced adipocyte differentiation. Cell lysates were corrected at d 7. C, Staining of neutral lipids by Oil Red O. *Upper panel* is the amount of neutral lipid as determined by measurement at OD 490. D, Expression of genes associated with adipose differentiation (n = 3). **, $P < 0.01$; *, $P < 0.05$ compared with negative control siRNA.

protein (Fig. 3B) of several target genes 48 h after transfection. After this time, differentiation media were added to the cells, and differentiation allowed to proceed normally. Seven days after induction of differentiation, neutral lipid content stained with Oil Red O was reduced markedly in cells receiving Angptl2 siRNA treatment compared with negative controls (Fig. 3C). Expression of adipocyte differentiation marker genes, including aP2, Adipoq, peroxisome proliferator-activated receptor (PPAR)α, PPARγ, and CCAAT-enhancer-binding proteins (CEBPα and CEBPβ) (Fig. 3D), were also reduced in cells receiving Angptl2 siRNA treatment compared with negative controls. However, treatment with 1 mg/ml Angptl2 during differentiation did not affect the degree of differentiation (Supplemental Fig. 4). Angptl2 is highly expressed in 3T3-L1 adipocytes, and the differentiation medium was not changed for 2–3 d to induce adipocyte differentiation. Therefore, we believe that the amount of secreted Angptl2 in the culture medium of PBS-treated cells was sufficient to induce differentiation in these cells. These results also suggest that Angptl2 is not an aggressive inducer but rather an auxiliary factor in adipocyte differentiation.

Angptl2 increases insulin sensitivity by stimulating insulin-dependent phosphorylation of Akt and its substrates but not IRS or ERK1/2

To investigate the effects of Angptl2 on adiponectin expression, we transfected 3T3-L1 adipocytes with Angptl2 siRNA. This was effective in reducing the expression of Angptl2 mRNA and protein (Fig. 4A). Treatment with Angptl2 siRNA also decreased the expression of adiponectin mRNA, and correspondingly, we also observed that the concentration of adiponectin protein in the culture medium was reduced (Fig. 4B). Moreover, treatment with 1 μg/ml Angptl2 for 72 h increased the expression and release of adiponectin in 3T3-L1 adipocytes (Fig. 4C). Akt is a key molecule in insulin-dependent glucose uptake (17). A crucial event in this process is the translocation of GLUT4 (SLC2A4) to the plasma membrane, a process which acts as a regulator of glucose uptake in cells. This trafficking process is mediated, in part, as a result of

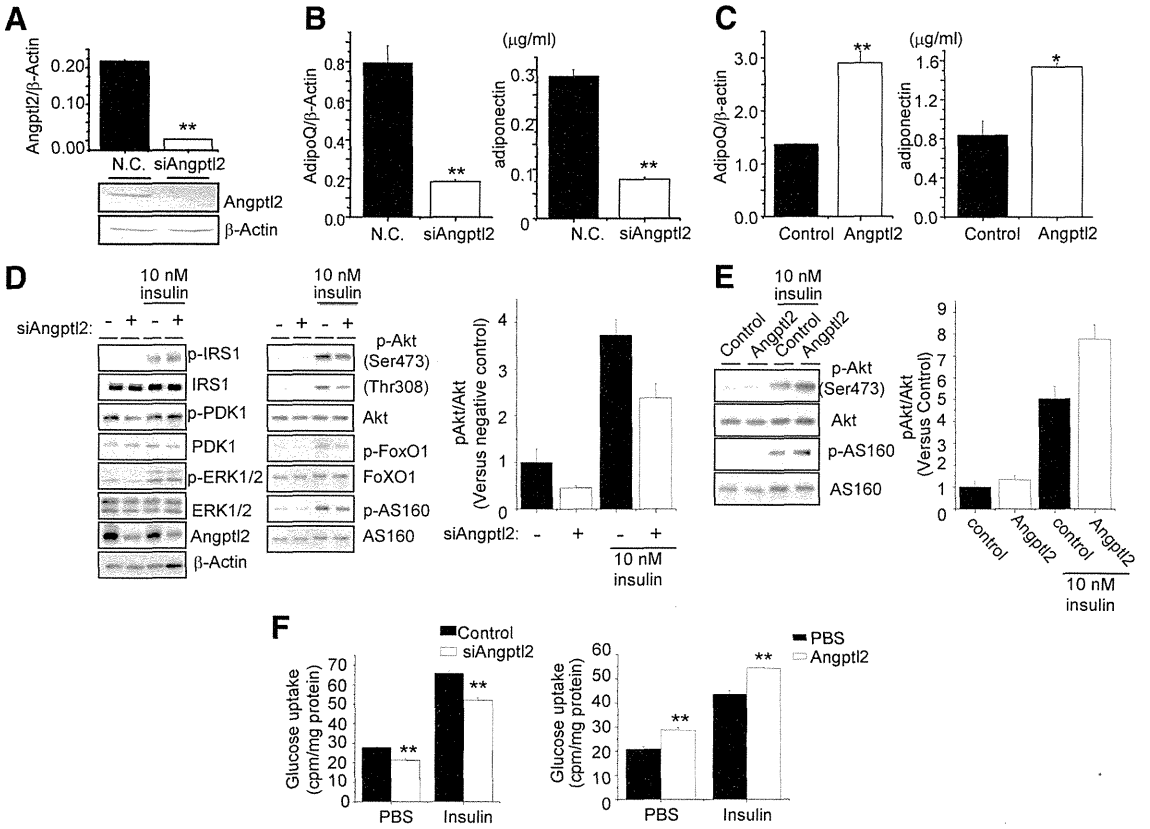

FIG. 4. Effects of Angptl2 on insulin sensitivity in 3T3-L1 adipocytes. A, Effects of Angptl2 siRNA on expression of mRNA (*left panel*) and protein (*right panel*) (n = 3). B and C, Levels of adiponectin mRNA expression and protein concentration in culture medium of 3T3-L1 adipocytes treated with or without Angptl2 siRNA (B) or recombinant Angptl2 (C) (n = 4). For treatment with recombinant Angptl2, the culture medium with or without 1 μg/ml Angptl2 was changed every day for 3 d. D and E, Effects of Angptl2 siRNA (D) and 1 μg/ml recombinant Angptl2 (E) on phosphorylation levels of insulin signaling molecules, determined by immunoblotting. The graph represents the ratio of band densities, comparing phosphorylated Akt to total Akt protein (n = 3). F, Effect of Angptl2 siRNA (*left*) and 1 μg/ml recombinant Angptl2 (*right*) on insulin-induced glucose uptake (n = 3). **, $P < 0.01$; *, $P < 0.05$ compared with negative control siRNA or PBS control. N.C., Negative control.

AS160 phosphorylation by Akt (18). To examine the effects of Angptl2 on insulin-induced activation of the Akt signaling pathway, we measured the phosphorylation levels of insulin signaling proteins. Treatment with Angptl2 siRNA inhibited insulin-induced phosphorylation of Akt and several Akt substrates, including FoxO1 (19) and AS160 (Fig. 4D). However, phosphorylation of IRS-1 and pyruvate dehydrogenase kinase 1, which are upstream of Akt, and of ERK1/2, another insulin signaling pathway, was not influenced by treatment with Angptl2 siRNA (Fig. 4D). Similar results were obtained using two other Angptl2 siRNA (Supplemental Fig. 5). In addition, treatment with 1 μg/ml Angptl2 enhanced the insulin-induced phosphorylation of Akt, FoxO1, and AS160 (Fig. 4E). Similarly, insulin-induced glucose uptake was decreased by treatment with Angptl2 siRNA, whereas glucose uptake was increased by treatment with 1 μg/ml Angptl2 (Fig. 4F).

Angptl2 regulates Akt activity as a result of reduced Trib3 expression

Phosphorylation of IRS-1 and pyruvate dehydrogenase kinase 1, which are upstream of Akt, and of ERK1/2, another insulin signaling pathway, was not influenced by treatment with Angptl2 siRNA. This result suggests that Angptl2 influences an Akt-specific regulatory protein. Therefore, we investigated whether Angptl2 affected the expression of Trib3, a specific Akt inhibitory protein (20). Trib3 mRNA expression was increased by Angptl2 siRNA treatment and decreased by treatment for 48 h with 1 μg/ml Angptl2 (Fig. 5A). The expression of Trib3 protein was also increased by Angptl2 siRNA treatment (Fig. 5B). To investigate the relationship between Trib3 and Angptl2-regulated insulin resistance, we cotransfected Trib3 siRNA with Angptl2 siRNA. The suppression of Akt phosphorylation caused by treatment with Angptl2 siRNA was partially recovered by cotransfection with Trib3 siRNA (Fig. 5C). Meanwhile, the enhanced insulin-induced phosphorylation of Akt by Angptl2 treatment was not observed in cells treated with Trib3 siRNA (Fig. 5D). Furthermore, expression of adiponectin mRNA was also increased by Trib3 siRNA (Fig. 5E). These data indicated that Angptl2 partially increased insulin sensitivity via reduced Trib3 expression in 3T3-L1 adipocytes. We then examined expression of Trib3 in adipose tissues ad-

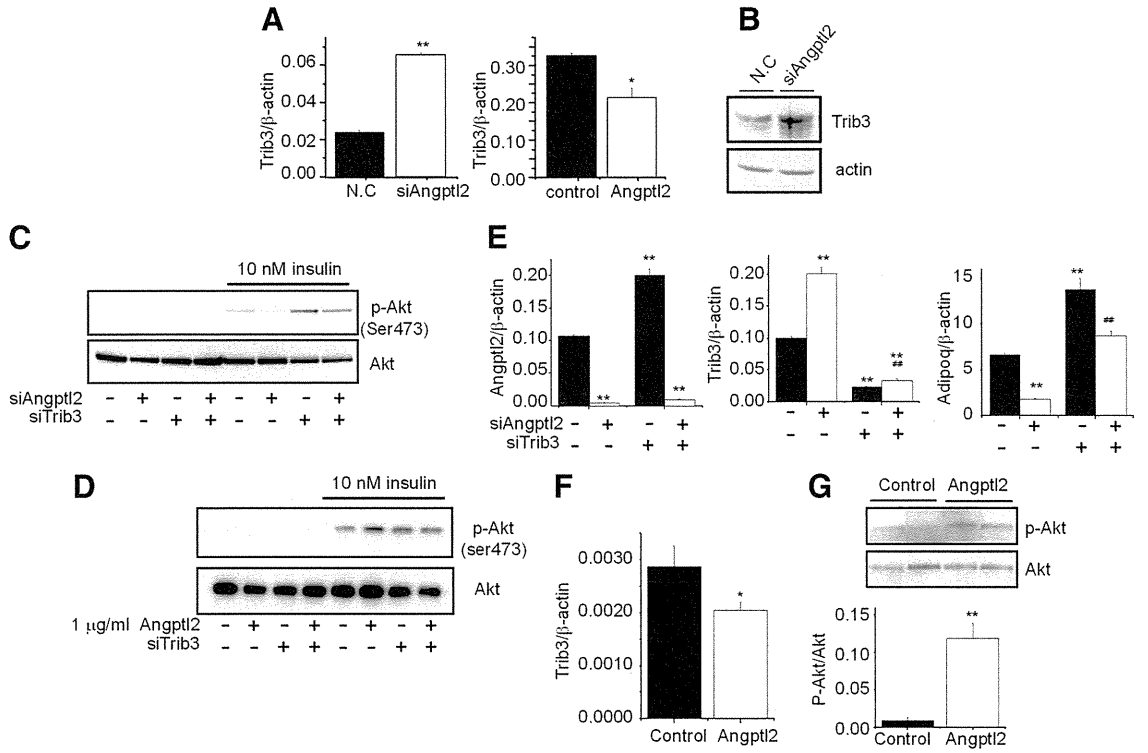

FIG. 5. Effects of Trib3 on Angptl2-induced stimulation of insulin sensitivity. A and B, Levels of Trib3 mRNA (A) and protein (B); n = 3 per group. C, Effects of cotransfection of Angptl2 and Trib3 siRNA on insulin-induced Akt phosphorylation. D, Effect of Trib3 siRNA on recombinant Angptl2-induced stimulation of insulin-dependent Akt phosphorylation. E, Effect of Trib3 siRNA on Angptl2 siRNA-induced reduction in adiponectin mRNA. F, Levels of Trib3 mRNA in mesenteric adipose tissues of mice administered with 0.8 mg/kg body weight per day Angptl2 or PBS at ZT12 for 4 wk (n = 5). G, Levels of phosphorylated Akt in mesenteric adipose tissues 2 h after final administration of Angptl2 or PBS, determined by Western blotting (*upper panel*). The graph represents the ratio of band densities, comparing phosphorylated Akt to total Akt protein (*lower panel*) (n = 3). **, $P < 0.01$; *, $P < 0.05$ compared with negative control siRNA or PBS control. N.C., Negative control.

ministrated with Angptl2. In adipose tissues of mice administrated Angptl2, the expression of Trib3 was reduced (Fig. 5F), and phosphorylated Akt was increased 2 h after the final administration (Fig. 5G).

Discussion

In this study, we observed circadian expression of Angptl2 in epididymal adipose tissue, with the peak phase occurring at ZT12. This peak phase was consistent with the active period of feeding behavior, and the rhythmic expression was disrupted after the weight gain and insulin resistance by reduced gene expression during the peak phase. It was notable that the administration of Angptl2 to *db/db* mice during the peak period of expression reduced plasma glucose, insulin, and lipid levels. The reductions of plasma insulin and lipid levels were observed at least for 12 h after administration (Supplemental Fig. 6). Furthermore, the difference in random-fed glucose level between PBS and Angptl2 group was gradually increased during 4-wk administration. These results suggested that treatment with Angptl2 improved glucose metabolism in organs/tissues and reduced plasma insulin level. Because of the improvement of hyperinsulinemia, excessive fat synthesis and lipid storage might be suppressed in liver and adipose tissues of Angptl2-treated mice. To investigate whether this reduction was possibly, due to improvements in insulin sensitivity, we examined the effects of Angptl2 on insulin sensitivity in 3T3-L1 adipocytes. We found that Angptl2 increased the expression of adiponectin and insulin-dependent glucose uptake by regulating insulin sensitivity in adipocytes. These results indicate that the effects of Angptl2 on glucose tolerance in *db/db* mice might be due to improvements in insulin resistance, although further *in vivo* studies are needed to confirm this finding.

An important component of nutrient homeostasis is the coordination of daily rhythms of rest and activity, feeding behavior, energy utilization, and energy storage across the 24-h light/dark cycle. Recent molecular studies observed 24-h variation in the expression of mRNA encoding several genes involved in energy homeostasis. In the liver, coordinated circadian expression of glucose transporters, the glucagon receptor, and enzymes involved in rate-limiting steps in the metabolism of hexose sugars have been reported, with the peak phase of expression occurring during the feeding period (21). Similarly, in adipose tissue, the